SILICON MATERIALS TASK OF THE LOW COST SOLAR ARRAY PROJECT (PHASE III)

DRD No. SE7
DRL No. 58

Dist. Category UC-63

DOE/JPL-954331-79/7

Effect of Impurities and Processing on Silicon Solar Cells

Fifteenth Quarterly Report

July, 1979

April 1979-June 1979

R. H. Hopkins, J. R. Davis, P. D. Blais,
A. Rohatgi, R. B. Campbell, P. Rai-Choudhury and R. E. Stapleton
Westinghouse Research & Development Center
and
H. C. Mollenkopf and J. R. McCormick
Hemlock Semiconductor Corporation

Contract No. 954331

The JPL Low Cost Silicon Solar Array Project is sponsored by the U. S. Dept. of Energy and forms part of the Solar Photovoltaic Conversion Program to initiate a major effort toward the development of low-cost solar arrays. This work was performed for the Jet Propulsion Laboratory, California Institute of Technology by agreement between NASA and DOE.

Westinghouse R&D Center
1310 Beulah Road
Pittsburgh, Pennsylvania 15235

TECHNICAL CONTENT STATEMENT

This report was prepared as an account of work sponsored by the United States Government. Neither the United States nor the United States Department of Energy, nor any of their employees, nor any of their contractors, sub-contractors, or their employees, makes any warranties, express or implied, or assumes any legal liability or responsibility for the accuracy, completeness or usefulness of any information, apparatus, product or process disclosed, or represents that its use would not infringe privately owned rights.

NEW TECHNOLOGY

No new technology is reportable for the period covered by this report.

TABLE OF CONTENTS

TABLE OF CONTENTS (Cont.)

LIST OF TABLES

LIST OF TABLES (Cont.)

LIST OF FIGURES

1. SUMMARY

The overall objective of this program is to define the effects of impurities, various thermochemical processes, and any impurity-process interactions on the performance of terrestrial silicon solar cells. The results of the study form a basis for silicon producers, wafer manufacturers, and cell fabricators to develop appropriate cost-benefit relationships for the use of less pure, less costly Solar Grade silicon.

We have performed the first reported determinations of the segregation coefficients of tungsten, tantalum, and cobalt for the Czochralski pulling of silicon single crystals. Sensitive neutron activation analysis was used to determine the metal impurity content of the silicon (C_S) while atomic absorption was used to measure the metal content of the residual liquid (C_L) from which the doped crystals were grown. The effective segregation coefficients computed from the relation $k_{eff} = C_S/C_L$ were $k_W = 1.7 \times 10^{-8}$, $k_{Ta} = 2.1 \times 10^{-8}$ and $k_{Co} = 1 \times 10^{-5}$. The previously reported value $k_{Mo} = 4.5 \times 10^{-8}$ was also confirmed.

Gettering of Ti-doped silicon wafers improves cell performance by 1 to 2% (absolute) for the highest temperatures and longest times. $HC\ell$ is more effective thar $POC\ell_3$ treatments for deactivating Ti but $POC\ell_3$ and $HC\ell$ produce essentially identical results for Mo or Fe. Detailed analysis by deep level transient spectroscopy (DLTS) indicates that the performance improvement is due to a reduction in the number of active recombination centers not to a change in the recombination energy level. The reduction in trap center density is not uniform through a silicon wafer, but is lowest near the phosphorus-rich junction region then increases with distance into the wafer eventually becoming constant at a value equal to that in the bulk material before the gettering operation.

The measured profile for Ti centers formed after an 850°C gettering operation was fitted by a mathematical expression for the out-diffusion of an impurity species. From the fit of the data we calculated a diffusion constant $D_{Ti} \sim 1.27 \times 10^{-11}$ cm^2/sec, a value close to that extrapolated from high temperature data in the literature. Gettering data for Mo imply that this impurity diffuses much more slowly in silicon than does Ti.

By means of cell performance data and the newly-measured segregation coefficients we have computed curves to predict the variation in cell efficiency with impurity concentration for Mo, Ta, W, Nb and Co, materials commonly employed in the construction of high temperature silicon processing equipment. Co behaves much like Mn and Fe producing only modest performance degradation. In contrast Mo, Ta, W and Nb all degrade cell performance severely.

Using data for second and third generation n-base ingots we updated the cell performance curves for single impurities in n-type silicon. Most impurities degrade n-base cells less than p-base devices. The effect is largest for Mo, Al, Mn, Ti and V while Fe and Cr behave much the same in both types of solar cells. In contrast Ni and Cu both degrade n-base devices (apparently by a junction mechanism) more severely than p-base cells.

2. INTRODUCTION

This is the 15th quarterly report describing activities conducted under JPL Contract 954331. Phase III of this program is entitled "An Investigation of the Effects of Impurities and Processing on Silicon Solar Cells."

The objective of this program is to determine how thermal processes, impurities, and impurity-process interactions affect the properties of silicon and the performance of terrestrial solar cells made from silicon. The development of this data base permits the definition of the tolerable impurity levels in a low-cost Solar Grade Silicon. In addition, the data provide the silicon manufacturer with a means to select materials of construction which minimize product contamination and permit the cost-effective selection of chemical processes for silicon purification. For the silicon ingot, sheet, or ribbon manufacturer, the information indicates what silicon feedstock purity must be selected to produce wafers suitable for cell production and what furnace materials minimize wafer contamination. The cell manufacturer may use the impurity-cell performance relationships to define an acceptable wafer purity for cell fabrication and the heat treatment data to identify processes which minimize impurity impact on efficiency. In short, the impurity data provide a basis for cost-benefit analysis to the producers and users of Solar Grade Silicon.

The Phase III effort encompasses five major topics, several of which represent new directions for our work: (1) examination of the interaction of impurities with processing treatments, (2) generation of a data base and modeling of impurity effects in n-base solar cells, (3) extension of previous p-base studies to include impurities likely to be introduced during silicon production, refining or crystal growth, (4) a consideration of the potential impact of anisotropic (nonuniform) impurity distribution in large Czochralski and ribbon solar cells and,

(5) a preliminary investigation of the permanence of impurity effects in silicon solar cells.

During this past quarter experimental activity proceeded in each of the five task areas: (1) The effect of HCℓ high temperature treatment on the electrical activity of Ti, Mo and Fe was determined; detailed analysis of gettering mechanisms was performed and modeling of the impurity behavior was initiated, (2) solar cells on n-base material were fabricated and tested and model coefficiencts for the impurity-performance relations were derived, (3) further data describing the effects of Ta, W, Nb, and Co on solar cell performance were gathered and analyzed, (4) 7.6 cm diameter ingots doped with Fe and Cu and 3 to 4 cm wide silicon webs doped with Ti and V were grown to evaluate the effects of potential non-uniform impurity distributionsand (5) aging treatments on Ti and Mo doped cells were extended to 900°C; aging studies of Cr-doped ingots were initiated.

The highlights of these studies are described in the following sections of the report.

3. TECHNICAL RESULTS

3.1 Growth and Evaluation of Silicon Ingots

Major objectives of this activity have been to provide ingots purposely contaminated with controlled additions of metal impurities for subsequent electrical and solar cell evaluation and also to assess the effects of impurities on ingot microstructure. During this quarter, in addition to the preparation and analysis of the metal-doped Czochralski ingots, we have also made the first direct measurements reported for W and Ta segregation coefficients, updated segregation data for Mo and Co and determined the critical Nb, Cr and Fe concentrations at which the loss of single crystal structure occurs.

3.1.1 Segregation Coefficients of Transition Metals

As we have pointed out before,[1,2] conventional spark source mass spectrometry (SSMS) and neutron activation analytical (NAA) methods lack sufficient sensitivity to detect elements such as W, Ta, and Mo which, because of their relatively small segregation coefficients, are present only at low levels in silicon single crystals. Nevertheless, these elements even at low concentrations have profound effects on solar cell performance.[1,2] A fourth element, Co, can be detected by SSMS but the analysis of the data is hindered by the background from nearby silicon lines. Special techniques to extract the concentration data can be employed[3] but this approach increases the uncertainty in the analytical result. For this reason ingots bearing these impurities were subjected to sensitive NAA at the Kraftwerk Union.[1] We give here a preliminary report of the data; a more detailed evaluation will follow.

In Table 1 are compiled the most current values we have derived for the segregation coefficients of impurity elements in silicon crystals produced by Czochralski pulling. With the exception of Mo, Ta, W, Co

and Nb, the data represent the weighted averages of many samples analyzed by SSMS, conventional NAA and sensitive NAA.[1,2] In the case of Mo two analytical data points both from Kraftwerk Union (and in close agreement with each other) were used to derive the value $k_{Mo}=4.5\times10^{-8}$. For Ta and W the values $k_{Ta}=2.1\times10^{-8}$ and $k_{W}=1.7\times10^{-8}$ are each calculated on the basis of one analytical measurement by sensitive NAA. The similarities in magnitude for the segregation coefficients of Mo, Ta, and W might be expected on the basis of the proximity of the elements in the Periodic Table, a fact which gives further credibility to the analytical result.

Previously we had derived a value of 3.7×10^{-6} for the segregation coefficient of Co in silicon. The result was somewhat compromised by the high silicon background on the SSMS plate.[3] Sensitive NAA places the Co segregation coefficient at 1×10^{-5} as listed in Table 1. We adopted the latter result, based on our judgement of the relative uncertainties in the SSMS and NAA values. Moreover, the new value for Co is more consistent with the segregation coefficients of Mn, Fe, and Ni to which Co is chemically similar.

Finally,we have estimated a value of about 10^{-7} for Nb based primarily on its position relative to Ta and V, its neighbors in the Periodic Table. (We have not yet been able to detect Nb by SSMS in even the most heavily doped ingot, W-167. This places an upper limit of 1.5×10^{14} cm^{-3} on the ingot concentration. We plan to attempt a slower growth rate to increase the Nb concentration without causing ingot structure breakdown).

3.1.2 Ingot Structural Breakdown Via Constitutional Supercooling

We continue to compile data relating ingot structure to the contamination level of the silicon feedstock from which the ingot is grown. This information will be used in a detailed assessment of the cost-benefit tradeoff for solar grades of silicon (see, e.g. Reference 1).

Table 1. Segregation Coefficients

Element	Segregation Coefficient
Al	3×10^{-2} (2.8×10^{-3})
B	0.8
C	0.05
Ca	?
Cu	8.0×10^{-4}
Cr	1.1×10^{-5}
Fe	6.4×10^{-6}
Mg	3.2×10^{-6}
Mn	1.3×10^{-5}
Mo	4.5×10^{-8}
Ni	3.2×10^{-5}
Ph	0.35
Ta	2.1×10^{-8}
Ti	2.0×10^{-6}
V	4×10^{-6}
Zn	10^{-5}
Zr	$<1.6 \times 10^{-8}$
Co	1.0×10^{-5}
W	1.7×10^{-8}
Nb	$\sim 10^{-7}$

It is well established that when the liquid impurity concentration exceeds a critical value C_{ℓ}^{*} single crystal structure breaks down via constitutional supercooling[1,2] to a cellular-polycrystalline morphology. Increasing the crystal pulling rate or the crystal diameter reduces at crtical concentration for the onset of structural degradation.

In Figure 1, we show curves describing the expected variation in C_{ℓ}^{*} with growth speed overlaid with measured data for ingots doped with Nb, Cr and Fe, respectively. As for other impurities we have studied, the transition to cellular structure occurs at impurity concentrations in the mid $10^{20}cm^{-3}$ range.[1,2] Note the data point for Fe (ingot W-173) is for a 3.8 cm radius ingot and falls below the points for the 1.6 cm ingots bearing Nb and Cr. This would be expected due to the reduced thermal gradient in the larger size ingots.

3.1.3 Ingot Preparation

Sixteen ingots (W172 to W188, inclusive) were grown by Czochralski pulling during this quarter, using the same techniques and conditions described in previous reports.[1,2] Six of these were second, third and fourth generation ingots doped with boron and either Co, Nb, Ta or W to assess the impact of materials of construction on solar cell performance. The rest of the ingots were designated for compensation studies, gettering and heat treating experiments and to complete our data base on impurity effects in n-base silicon solar cells.

As in the past we have collected the analytical data for all ingots in Appendix 1. Listed there are the ingots, the target impurity concentrations, impurity concentrations based on melt analyses and measured impurity concentrations (SSMS).[2,4] Table 2 lists our best estimate of the impurity concentration in each of the ingots grown for the Phase III study. Note that these estimates have been revised to reflect the new values for the segregation coefficients of W, Co, and Ta. The estimated Nb concentrations are based on the assumption $k_{Nb} \sim 10^{-7}$.

Curve 71-943-A

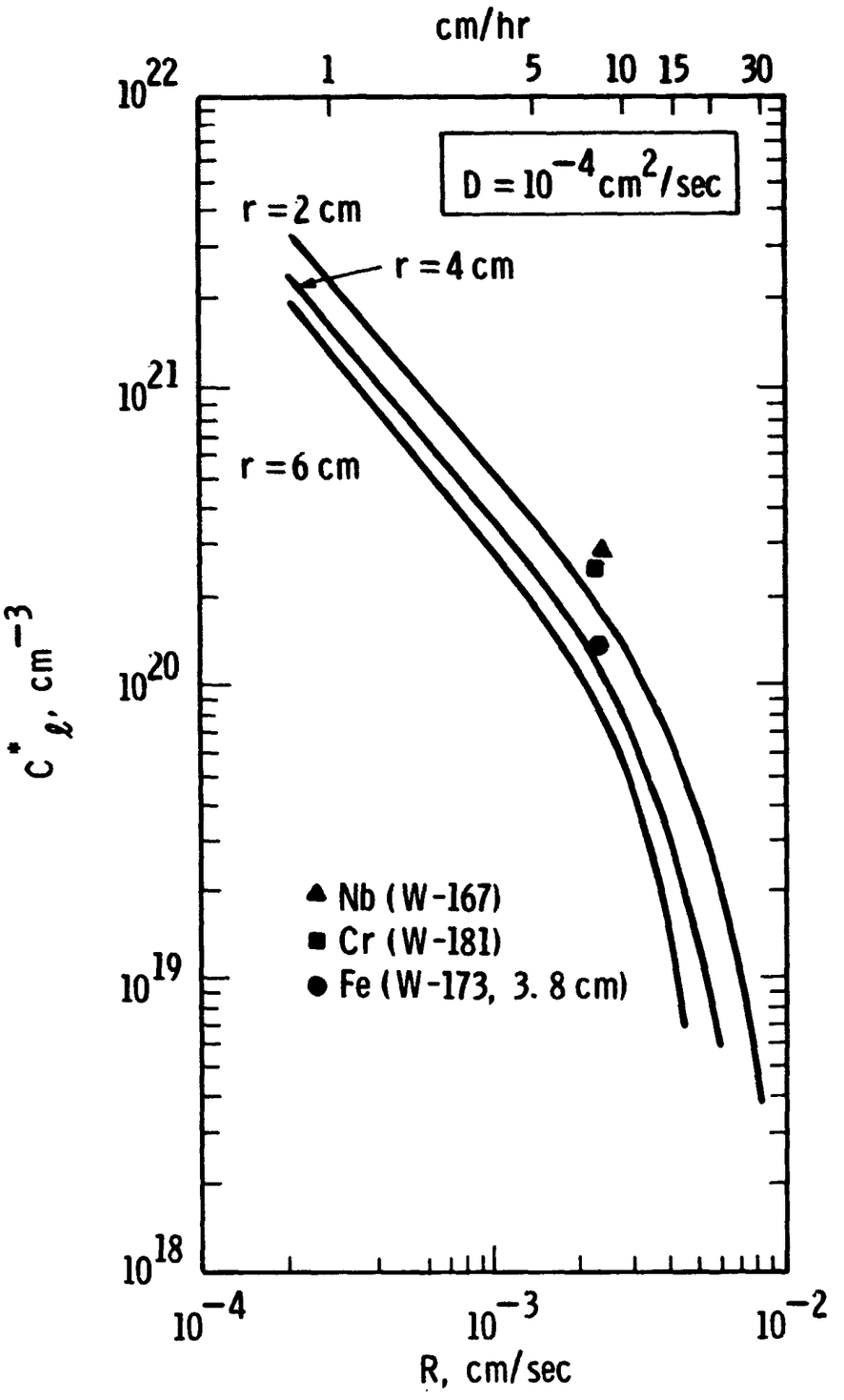

Figure 1 Predicted variation of critical liquid impurity concentration for crystal breakdown with crystal growth velocity during Czochralski pulling of silicon. Data points represent impurity concentrations at which breakdown actually took place (curves assume heat loss to o°K environment, see Reference 2)

Table 2. Best Estimate of Impurity Concentrations

Ingot Identification	Best Estimate of Impurity Concentration ($X10^{15}$ atoms/cm^3)
W-129-00-000 (7.6 cm)	NA
W-130-00-000 (7.6 cm)	NA
W-131-Mn-008 (7.6 cm)	0.55
W-132-Ta-003	0.000042
W-133-00-000	NA
W-134-Ti-009	0.03
W-135-Fe-005	0.78
W-136-Fe-006	0.24
W-137-Ti-010	0.21
W-138-Mo-005	0.001
W-139-Mo-006	0.0042
W-140-Ti-001 (7.6 cm)	0.18
W-141-Mo/Cu-001	0.004/4.00
W*-142-00-000	NA
W*-143-Ti-002	0.20
W-144-Mo-001	0.004
W-145-W-001	0.00085
W-146-Co-001	1.5
W-147-N/Ni-002	0.33
W-148-N/Mn-002	0.60
W-149-N/Fe-003	0.60
W-150-N/V-003	0.03
W**-151-00-000	NA
W**-152-Ti-001	0.21
W-153-N/Ti-003	0.013

Table 2. Best Estimate of Impurity Concentrations (Continued)

Ingot Identification	Best Estimate of Impurity Concentrations ($X\ 10^{15}$ atoms/cm^3)
W-154-N/Cr-003	0.50
W-155-N/Mo-001	0.001
W-156-N/Nb-002	0.004
W-157-N/Ti/V-001	0.08/0.12
W-158-N/Ti/V/Cr-001	0.05/0.05/0.55
W-159-N/Cr/Mn/Ti/V-001	0.35/0.32/0.02/0.02
W*-160-Ti-001	0.17
W**-161-Ti-002	0.03
W-162-Ni/Ti-001	1.21/0.16
W-163-Ni/V-001	1.0/0.44
W-164-Ni/Mo-001	1.23/0.004
W-165-Co-002	0.3
W-166-Fe-007	1.06
W-167-Nb-001	0.01++
W*-168-Ph-002	110+
W*-169-Ph-004	136+
W-170-Ph-005	150+
W-171-W-002	0.0015
W-172-Cu-006 (7.6 cm)	24
W-173-Fe-008 (7.6 cm)	0.51
W-174-Ta-004	0.00084
W-175-W-003	0.00027
W-176-00-000	NA
W-177-N/Cr/Mn-001	1.20/1.26
W-178-N/Mn/Ti-001	0.86/0.08
W*-179-Ph-006	NA
W*-180-Ti-00	0.13
W-181-Cr-006	1.04
W-182-Cr-007	0.45
W-183-Nb-002	0.002++

Table 2. Best Estimate of Impurity Concentrations (Continued)

Ingot Identification	Best Estimate of Impurity Concentrations ($X\ 10^{15}$ atoms/cm^3)
W-184-Pd-001	Processing
W-185-Cu/Ti-004	Processing
W-186-Co-003	Processing
W-187-Co-004	Processing

* Asterisk indicates low resistivity p-type ingot ($\leq$ 1 ohm-cm)
** 30 ohm-cm p-type ingot
\+ Value based on resistivity measurement
++ Assumed k value near 1×10^{-7}

3.1.4 Ingot Evaluation

The resistivity and etch pit density for each ingot continue to fall close to the norms established in Phases I and II of this program. The resistivity and etch pit data for ingots W-129 through W-187 are listed in Table 3.

The carbon and oxygen concentrations of each odd numbered ingot were measured by infrared absorption. The amplitude of the absorption peaks at 606 cm^{-1} and 1107 cm^{-1} is proportional to the carbon and oxygen concentrations, respectively. The constants of proportionality used in these measurements were 2.2 for carbon and 9.6 for oxygen[2]. We note that normal carbon and oxygen concentrations in Czochralski-grown material range from 2.5 to 50×10^{16} atoms/cm^3 for carbon, and from 5 to 150 x 10^{16} atoms/cm^3 for oxygen; no significant deviations from these values were observed in the ingots produced this quarter, viz. Table 4.

3.2 Processing Studies

Elevated temperature treatment of contaminated silicon wafers in an ambient bearing $POCl_3$ or HCl provides one way to electronically deactivate, or getter, the impurities after an ingot is grown. Thus we may improve the performance of solar cells fabricated from solar grades of silicon with an appropriate thermochemical process. We have carried out a series of experiments to delineate the time-temperature and chemical species response for a number of impurities which degrade cell performance. The improvements in cell performance for $POCl_3$ treatments were described previously;[3] recent results in which HCl was employed to effect gettering are discussed here. We also report some extensions to the $POCl_3$ experiments; detailed examinations of these results by deep level transient spectroscopy (DLTS), and model calculations of impurity gettering.

3.2.1 Thermochemical Behavior of Impurities in Silicon

3.2.1.1 Impurity Gettering by High Temperature HCl Treatment

Our first experiments with HCl as a gettering medium utilized the same five impurity-doped ingots as in the $POCl_3$ investigations:[3]

Table 3 Resistivity and Etch Pit Density of Phase III Ingots

Ingot Identification	TGT Resistivity (ohm-cm)	Actual Resistivity (ohm-cm)	Etch+ Pit Density (/cm^2)
W-129-00-000 (7.6 cm)	4.0 (B)	4.7-3.0	1 K-Gross Lineage
W-130-00-000 (7.6 cm)	4.0 (B)	4.7-3.7	OK-Gross Lineage
W-131-Mn-008 (7.6 cm)	4.0 (B)	6.0-3.8	OK-Gross Lineage
W-132-Ta-003	4.0 (B)	3.8-3.4	1-20K
W-133-00-009	4.0 (B)	4.3-3.7	OK-Gross Lineage
W-134-Ti-009	4.0 (B)	4.9-4.4	0-10K
W-135-Fe-005	4.0 (B)	5.3-2.1	0-Gross Lineage
W-136-Fe-006	4.0 (B)	3.3-2.7	1K-Gross Lineage
W-137-Ti-010	4.0 (B)	4.6-4.4	0-Gross Lineage
W-138-Mo-005	4.0 (B)	5.0-4.1	0-5K
W-139-Mo-006	4.0 (B)	4.0-2.3	0-Gross Lineage
W-140-Ti-011 (7.6 cm)	4.0 (B)	3.6-1.7	5K-Gross Lineage
W-141-Mo/Cu-001	4.0 (B)	4.7-3.0	2K-Gross Lineage
W*-142-00-000	0.2 (B)	0.22-0.20	0-3K
W*-143-Ti-002	0.2 (B)	0.21-0.15	0-Gross Poly
W*-144-Mo-001	0.2 (B)	0.23-0.19	0-Gross Poly
W-145-W-001	4 (B)	4.5-4.0	2K-Gross Poly
W-146-Co-001	4 (B)	4.7-4.2	1K-Gross Poly
W-147-N/Ni-002	1.5 (P)	1.9-1.4	2-15K
W-148-N/Mn-002	1.5 (P)	2.5-2.1	1K-Gross Poly
W-149-N/Fe-003	1.5 (P)	2.0-1.6	3K-Gross Poly
W-150-N/V-003	1.5 (P)	2.0-1.5	1-5K
W*-151-00-000	30 (B)	35.6-18.1	0-5K
W*-152-Ti-001	30 (B)	31.9-25	0-Gross Poly
W-153-N/Ti-003	1.5 (P)	2.1-1.1	0-10K
W-154-N/Cr-003	1.5 (P)	2.1-1.4	3K-10K
W-155-N/Mo-001	1.5 (P)	1.9-1.8	1-4K
W-156-N/Mo-002	1.5 (P)	1.7-1.3	3K-Gross Poly
W-157-N/Ti/V-001	1.5 (P)	2.0-1.6	1-10K
W-158-N/Ti/V/Cr-001	1.5 (P)	2.1-1.6	1K-gross Lineage
W-159-N/Cr/Mn/Ti/V-001	1.5 (P)	2.0-1.8	1-2K

Table 3 Resistivity and Etch Pit Density of Phase III Ingots (Continued)

Identification	TGT Resistivity (ohm-cm)	Actual Resistivity (ohm-cm)	Etch+ Pit Density (/cm^2)
W*-160-Ti-001	1.0 (B)	1.3-1.0	2-8K
W**-161-Ti-002	30 (B)	31.8-21.7	1-15K
W-162-Ni/Ti-001	4.0 (B)	4.5-4.0	OK-Clusters
W-163-Ni/V-001	4.0 (B)	4.8-4.4	1K-Clusters
W-164-Ni/Mo-001	4.0 (B)	4.7-3.2	OK-Clusters
W-165-Co-002	4.0 (B)	4.5-3.8	0-5K
W-166-Fe-007	4.0 (B)	4.7-3.0	OK-Gross Lineage
W-167-Nb-001	4.0 (B)	4.0-5.7	OK-Poly
W*-168-Ph-002	0.5 (B)	0.41-0.50	3-10K
W*-169-Ph-004	1.0 (B)	0.9-1.4	OK
W-170-Ph-005	2.9 (B)	1.1-2	1-3K
W-171-W-002	4.0 (B)	4.3-4.1	0-2K
W-172-Cu-006 (7.6 cm)	4.0 (B)	3.4-2.7	0-10K
W-173-Fe-008 (7.6 cm)	4.0 (B)	5.9-3.6	3K-Poly
W-174-Ta-004	4.0 (B)	4.3-3.8	OK-Twin
W-175-W-003	4.0 (B)	4.1-3.3	0-10K
W-176-00-000	2.0 (P)	2.0-1.3	OK
W-177-N/Cr/Mn-001	2.0 (P)	2.2-1.4	OK-Poly
W-178-N/Mn/Ti-001	2.0 (P)	2.1-1.7	2K-Poly
W*-179-Ph-006	0.35 (B)	0.3-0.3	0-2K
W*-180-Ti-001	0.5 (B)	0.51-0.49	2-5K
W-181-Cr-006	4.0 (B)	5.4-4.0	OK Clusters
W-182-Cr-007	4.0 (B)	4.2-3.6	0-4K
W-183-Nb-002	4.0 (B)	3.6-2.9	0-5K
W-184-Pd-001	4.0 (B)	4.2-3.9	0-4K
W-185-Cu/Ti-004	4.0 (B)	4.7-4.6	0-Poly
W-186-Co-003	4.0 (B)	4.1-3.7	0-2K
W-187-Co-004	4.0 (B)	3.8-2.9	Processing

see key on next page

Table 3 Resistivity and Etch Pit Density of Phase III Ingots (Continued)

* Low resistivity p-type ingot ($\leq$1 ohm-cm)

** Use of double asterisk indicates 30 ohm-cm p-type ingot.

\+ The first figure is etch pit density of the seed; second figure etch pit density of extreme tang end of ingot. The first value shown is indicative of dislocation density in slices used for cell fabrication. Structural degradation commonly occurs at the tang end of the most heavily-doped ingots due to constitutional supercooling. (1)

Table 4 Carbon and Oxygen Concentrations of Phase III Ingots

Ingot Number	Carbon Concentration x 10^{16} atoms/cm^3	Oxygen Concentration x 10^{16} atoms/cm^3
W-129-00-000	11.3	202
W-131-Mn-008	5.3	164
W-133-00-000	10.4	117
W-135-Fe-005	9.4	118
W-137-Ti-010	5.3	134
W-139-Mo-006	6.5	149
W-141-Mo/Cu-001	8.3	156
W*143-Ti-002	++	++
W-145-W-001	5.8	149
W-147-N/Ni-002	14.0	157
W-149-N/Fe-003	6.6	151
W**151-00-000 (30Ω-cm)	7.0	154
W-153-N/Ti-001	7.5	160
W-155-N/Mo-001	9.2	183
W-157-N/Ti/V-001	5.7	103
W-159-N/Cr-Mn/Ti/V-001	8.7	183
W**-161-Ti-002	6.0	138
W-163-Ni/V-001	5.0	128
W-165-Co-002	11.2	106
W-167-Nb-001	6.0	130
W*-169-Ph-004	14	96
W-171-W-002	10	86
W-173-Fe-008	Incomplete	Incomplete
W-175-W-003	10	158
W-177-N/Cr/Mn-001	8	150
W*-179-Ph-006	++	++
W-181-Cr-006	8	119
W-183-Nb-002	6	35
W-185-Cu/Ti-004	5	39
W-187-Co/-004	Processing	Processing

* low resistivity ingot
** high resistivity ingot
\+ Due to free carrier absorption infrared methods cannot be used for carbon and oxygen determination in these samples.

W 134 Ti 009

W 137 Ti 010

W 138 Mo 005

W 139 Mo 006

W 136 Fe 006

This approach facilitates comparison of the cell performance-gettering data from both types of experiments.

The experimental approach was similar to that employed before.[3] We subjected impurity-doped and uncontaminated baseline (Ingot W097) wafers to various time/temperature cycles in the presence of a 1% $HC\ell$-O_2 gas. After heat treatments, the wafers were cooled slowly to ambient temperature in order to preserve the bulk recombination lifetime. The gettered surface was etched from the wafers, and each was made into a solar cell via our standard process.[1,2] Testing the devices and analysis of the data completed the experiment.

So far wafers from the five impurity-doped ingots have been subjected to four thermal treatments: 1 hour at 1000°C and 1, 2 and 4 hours, respectively at 1100°C. The experimental data for each ingot are compiled in Tables 5 to 9 respectively. The trends of the data are more easily visualized with the aid of Figures 2 and 3, in which the normalized solar cell efficiency, η/η baseline, is plotted as a function of gettering temperature and gettering time, respectively.

It is clear that as gettering temperature (for a fixed time) is raised, cell performance improves, Figure 2. This is a result very similar to the behavior observed when $POC\ell_3$ was the gettering ambient.[3] We would also expect extending the gettering time at constant temperature to have a similar effect. This is true if one considers the extreme times, Figure 3. However the curves dip at 2 hours. The downward curvature in this plot is yet to be explained and is inconsistent with earlier $POC\ell_3$ experiments. Deep level spectroscopic and dark I-V measurements are underway in an effort to understand the apparent anomaly in isothermal data.

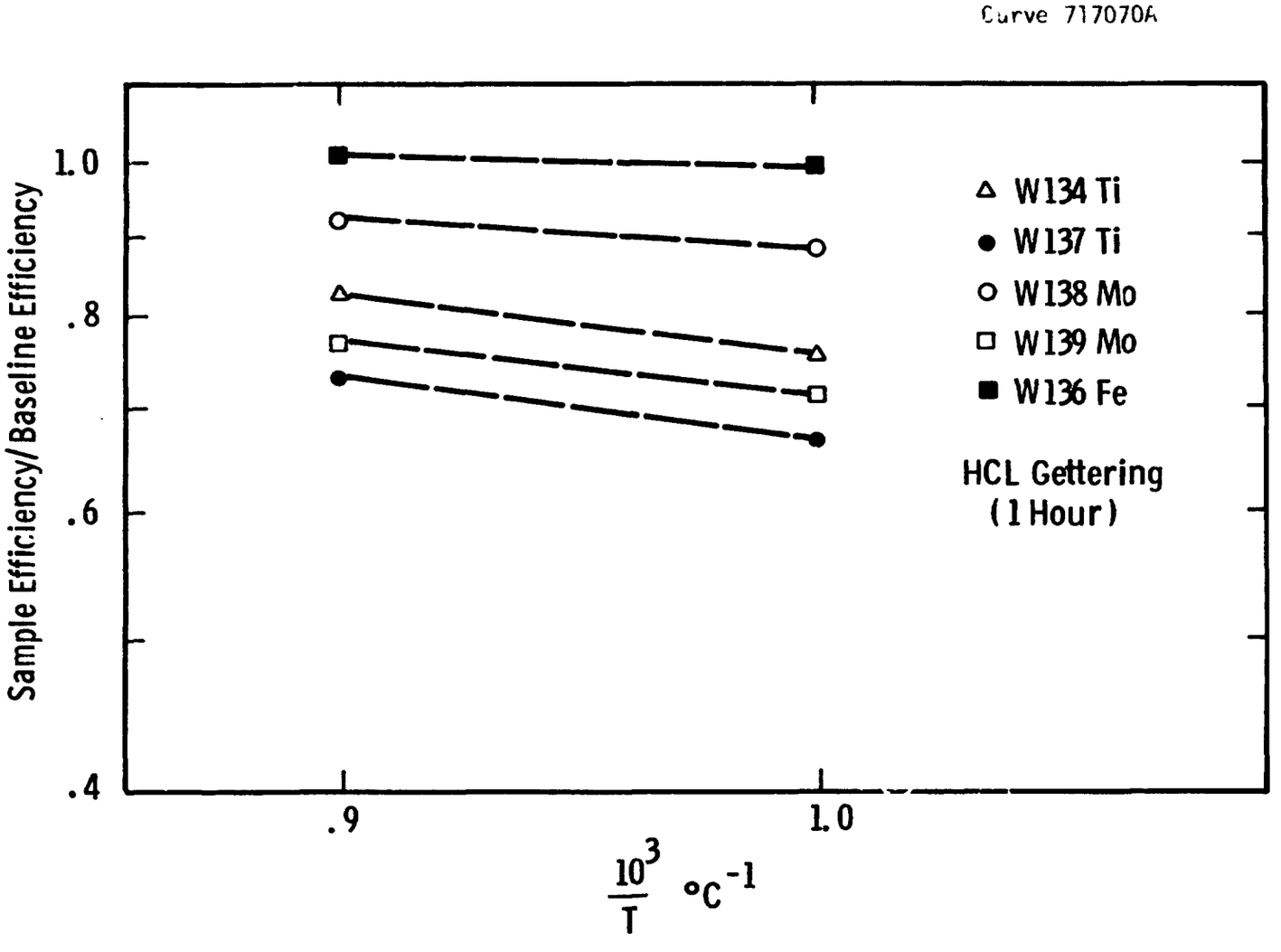

Figure 2 Normalized efficiency for Isochrmal HCℓ Gettering (1 Hr)

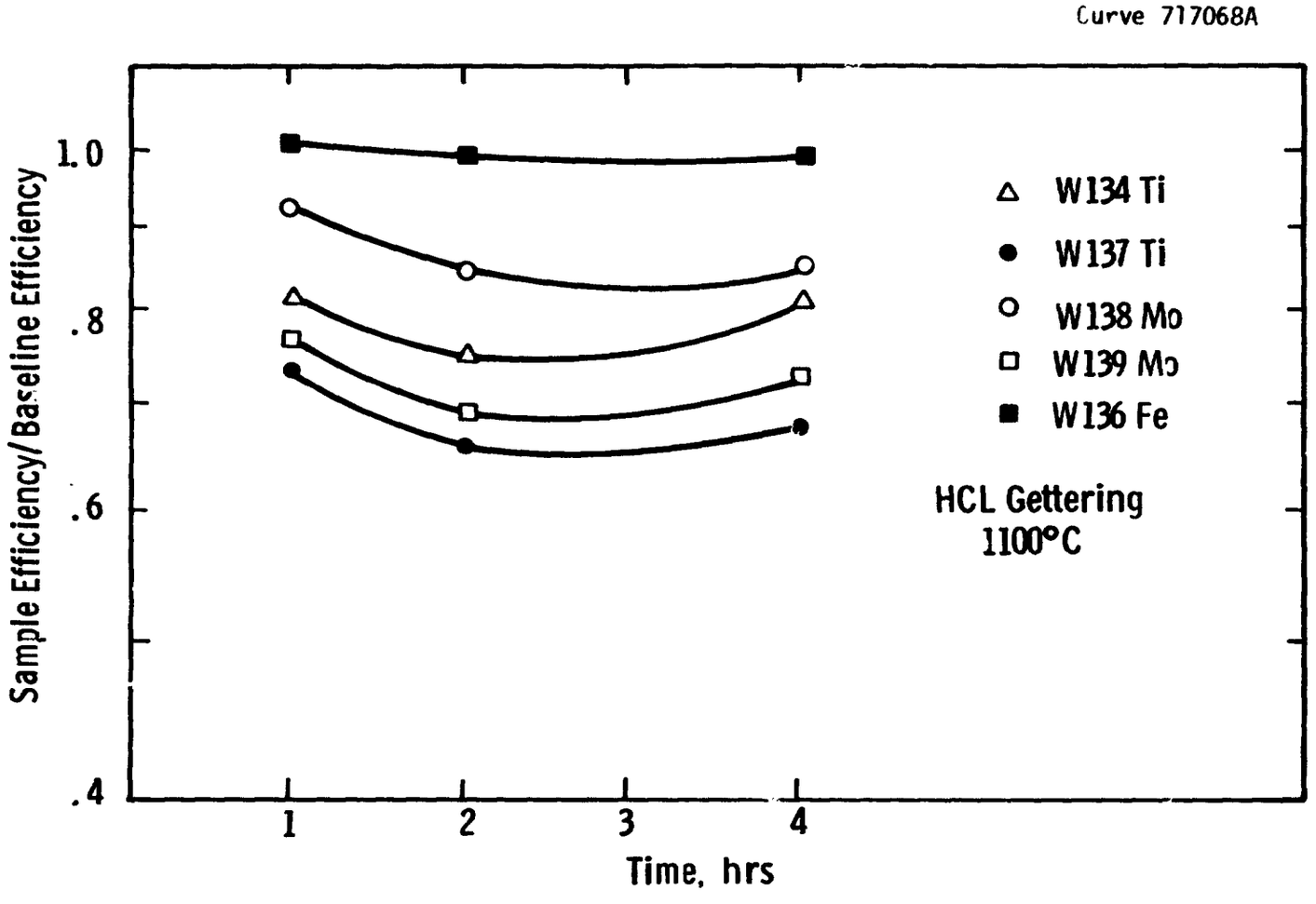

Figure 3 Normalized Solar Cell Efficiency as a Function of Gettering Time in HCl_x at 1100°C

TABLE 5

HCℓ GETTERING OF TI-DOPED SILICON

W134Ti009 Ingot

W097000 Baseline

	I_{sc}(mA)	V_{oc}(V)	FF	η(%)	τ_{ocd}(μsec)
1 HR @ 1000°C					
Base	21.55	.552	.733	9.20	4.0
Ingot	17.91	.520	.704	6.94	.5
Ingot/Base	.831	.942	.960	.754	.13
1 HR @ 1100°C					
Base	21.40	.543	.683	8.39	2.1
Ingot	18.04	.515	.690	6.77	.4
Ingot/Base	.843	.948	1.01	.807	.19
2 HRS. @ 1100°C					
Base	22.10	.556	.742	9.63	5.0
Ingot	18.58	.526	.705	7.37	.5
Ingot/Base	.841	.946	.950	.765	.10
4 HRS. @ 1100°C					
Base	22.00	.558	.718	9.33	4.5
Ingot	18.97	.533	.719	7.60	.7
Ingot/Base	.86	.955	1.00	.815	.15

TABLE 6

HCℓ GETTERING OF TI-DOPED SILICON

W137Ti-010 Ingot
W097000 Baseline

	I_{sc}(mA)	V_{oc}(V)	FF	η	τ_{ocd}(μsec)
1 HR. @ 1000°C					
Base	22.23	.553	.691	8.98	3.97
Ingot	16.31	.501	.695	6.00	0.84
Ingot/Base	0.734	.906	1.01	.668	.211
1 HR. @ 1100°C					
Base	21.2	.540	.668	8.09	2.08
Ingot	16.3	.498	.689	5.92	.58
Ingot/Base	.769	.922	1.03	.731	.279
2 HRS. @ 1100°C					
Base	22.17	.558	.74	9.77	4.46
Ingot	16.93	.511	.708	6.47	.60
Ingot/Base	.764	.916	.948	.662	.135
4 HRS. @ 1100°C					
Base	21.8	.558	.748	9.61	4.75
Ingot	17.28	.515	.700	6.58	.44
Ingot/Base	.793	.923	.936	.685	.093

TABLE 7

HCℓ GETTERING OF MO-DOPED SILICON

W138Mo-005 Ingot

W097000 Baseline

	I_{sc}(mA)	V_{oc}(V)	FF	η	τ_{ocd}(μsec)
1 HR @ 1000°C					
Base	21.30	.548	.735	9.07	3.25
Ingot	20.29	.524	.707	7.95	.95
Ingot/Base	.953	.956	.962	.877	.291
1 HR @ 1100°C					
Base	21.50	.546	.693	8.60	3.06
Ingot	20.09	.521	.706	7.83	1.04
Ingot/Base	.934	.954	1.02	.910	.339
2 HRS. @ 1100°C					
Base	22.40	.559	.729	9.65	4.94
Ingot	20.37	.528	.719	8.19	.94
Ingot/Base	.909	.949	.986	.849	.192
4 HRS. @ 1100°C					
Base	21.70	.554	727	9.24	4.03
Ingot	20.24	.528	.707	7.99	.92
Ingot/Base	.933	.953	.972	.862	.229

TABLE 8

HCℓ GETTERING OF MO-DOPED SILICON

W139Mo-006 Ingot
W097000 Baseline

	I_{sc}(mA)	V_{oc}(V)	FF	η	τ_{ocd}(μsec)
1 HR @ 1000°C					
Base	21.60	.550	.722	9.04	3.58
Ingot	18.09	.501	.666	6.39	.53
Ingot/Base	.838	.911	.922	.707	.149
1 HR @ 1100°C					
Base	21.75	.552	.736	9.33	4.75
Ingot	18.56	.506	.706	7.01	.74
Ingot/Base	.853	.917	.959	.751	.156
2 HRS. @ 1100°C					
Base	22.70	.563	.750	10.14	5.20
Ingot	18.65	.508	.700	7.02	.69
Ingot/Base	.822	.902	.933	.692	.133
4 HRS. @ 1100°C					
Base	21.80	.553	.721	9.19	4.30
Ingot	18.21	.508	.672	6.60	.541
Ingot/Base	.836	.919	.932	.718	.126

TABLE 9

HCl GETTERING OF Fe-DOPED SILICON

W136FE-006 Ingot

W097000 Baseline

	I_{sc}(mA)	V_{oc}(V)	FF	η	τ_{ocd}(μsec)
1 HR @ 1000°C					
Base	22.00	.550	.730	9.20	4.0
Ingot	21.95	.553	.711	9.12	3.6
Ingot/Base	.998	1.01	.974	.991	.90
1 HR @ 1100°C					
Base	21.65	.549	.715	8.97	4.0
Ingot	21.65	.549	.726	9.13	3.4
Ingot/Base	1.00	1.00	1.01	1.02	.85
2 HRS. @ 1100°C					
Base	22.0	.556	.746	9.78	4.5
Ingot	22.02	.562	.739	9.66	4.5
Ingot/Base	1.00	1.01	.978	.988	1.0
4 HRS. @ 1100°C					
Base	21.65	.557	.741	9.46	4.5
Ingot	21.50	.558	.738	9.36	3.5
Ingot/Base	.993	1.00	.996	.989	.778

The most significant aspect of the HCℓ gettering study becomes apparent when the HCℓ data and $POCℓ_3$ data are compared as in Figure 4. At any given temperature the HCℓ treatment is considerably more effective in reducing the harmful effects of Ti than is $POCℓ_3$. On the average the HCℓ gettered Ti-bearing cells are a full 1% (absolute) more efficient than cells subjected to $POCℓ_3$ treatment. In contrast HCℓ and $POCℓ_3$ treatments give similar results when either Mo or Fe are being gettered. Future studies will be aimed at identifying the reasons for the differences in impurity response and also extending the ranges of times and temperatures for HCℓ gettering.

As part of the HCℓ study a complementary set of experiments was carried out to evaluate the combined effect of back surface damage and HCℓ treatment on cell performance. Previous data suggested that damage enhanced the effectiveness of HCℓ gettering. Thus, one half the wafers in each run were lapped on one side with SiC grit prior to thermal treatment. We found no significant difference in performance between cells made on the damaged and undamaged wafers. Thus the data in Tables 5 to 9 and Figures 2 to 4 are the averages for all cells in a group.

3.2.1.2 Extension of $POCℓ_3$ Gettering Studies

Earlier we showed that for $POCℓ_3$ gettering, increasing the gettering time (constant temperature) or gettering temperature (fixed time) improved the performance of Ti and Fe doped solar cells; Mo-doped cells were only slightly affected. In these experiments the maximum temperature was 1100°C and the longest duration 4 hours.

To improve extrapolations of the data to wider temperature ranges we continued the $POCℓ_3$ studies by treating Ti-doped wafers for 1 hour at 1200°C. Following the treatment normalized cell efficiency rose to 0.58 from 0.51, the value for a 1 hour treatment at 1100°C. When the new data point is plotted on Figure2 of Reference 3 it falls on a smooth extension of the curve for ingot W137 Ti. Apparently the same gettering mechanism prevails over the interval from 850°C (cell diffusion) to 1200°C.

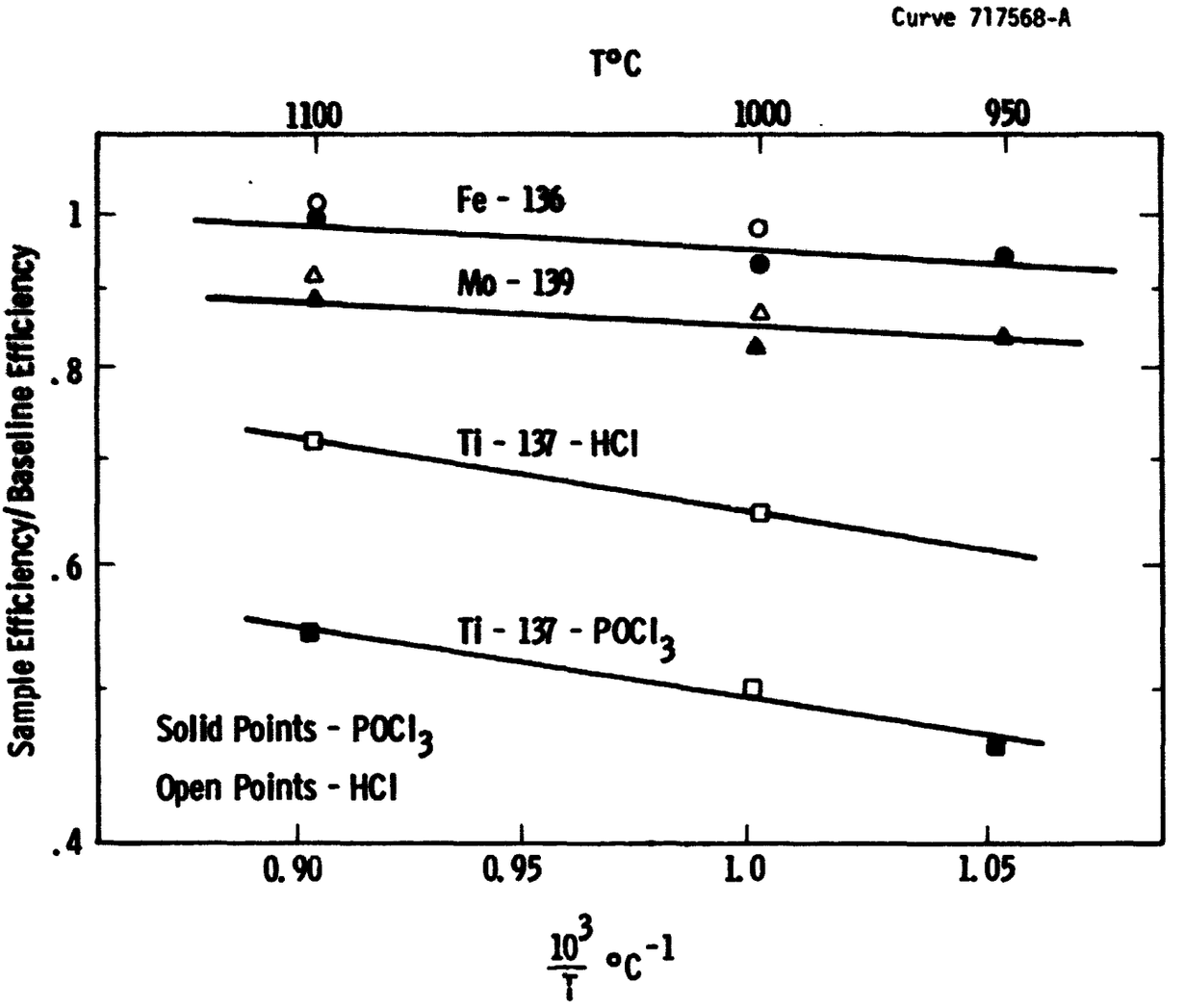

Figure 4 Comparison of normalized efficiency for isochronal $POCl_3$ and HCl gettering (1 hour)

3.2.2 Detailed Analysis of $POCl_3$ Gettering by Deep Level Spectroscopy

3.2.2.1 Ti-doped Silicon

In the last quarterly report we analyzed by DLTS the $POCl_3$ gettering of ingot W137Ti, a crystal doped with $2x10^{14} cm^{-3}$ Ti.[3] The gettering treatments ranged from 1 hour at 950°C to 5 hours at 1100°C. Since then we have completed DLTS measurements on wafers from the as-grown ingot and solar cells without any gettering. To accomplish the measurements thirty mil diameter Ti-Au Schottky barrier diodes were fabricated on the as-grown material. The recent results are compared with the earlier gettering data in Table 10.

We had established previously that $POCl_3$ gettering improved solar cell performance primarily by reducing the active Ti concentration (near the junction), not by altering the state of the Ti-induced recombination center at E_V+0.30eV. We find that the active Ti concentration in the as-grown wafer is about $7x10^{13}$ cm^{-3}, or nearly a factor of 3 less than the metallurgical Ti concentration. In contrast the active Ti concentration in the solar cell (near the junction) is only $1.76x10^{13}$ cm^{-3} (Table 10), a further reduction of about a factor of 4 in activity. This indicates that 825°C $POCl_3$ diffusion used for cell fabrication acts is an effective gettering step per se for Ti.

As the gettering intensity is increased from 950°C/1 hr. to 1100°C/5 hrs (prior to cell fabrication) the active concentration decreases systematically from $6.35x10^{12}$ cm^{-3} to $1.49x10^{12}$ cm^{-3}. Again we stress the need to recognize that DLTS measures the active impurity concentration in the depletion region, i.e. near the junction. If gettering produces an impurity profile in the wafer then the measured N_T will not represent the true active center density throughout the bulk. However, N_T will be related to the total number of recombination centers in the entire wafer.

TABLE 10

Variation in cell efficiency and trap concentration (N_T) as a function of gettering treatment for Ingot 137 (original metallurgical Ti concentration, $2.0 \times 10^{14} cm^{-3}$)

GETTERING CONDITION	NORMALIZED CELL EFFICIENCY (η/η_B), (%)	CONCENTRATION (N_T) OF E_V+0.30eV TRAP (cm^{-3})
None (starting wafer)		7.0×10^{13}
None (solar cell)	42.8	1.76×10^{13}
950°C/1 hr.	46.7	6.35×10^{12}
1000°C/1 hr.	51.0	3.94×10^{12}
1100°C/1 hr.	52.9	2.99×10^{12}
1100°C/2 hr.	55.4	2.50×10^{12}
1100°C/3 hr.	59.1	2.39×10^{12}
1100°C/5 hr.	66.2	1.49×10^{12}

For this reason we attempted to determine the concentration profile of electrically active Ti species in the as-grown wafer and also in solar cells subjected to no intentional gettering. The experiment was carried out as follows. The unprocessed wafer and the solar cell mesa were divided into 5 pieces. On each piece we etched steps ranging in depth from 2 to 10 μm. The step heights were measured with a Taly-step instrument (the corner of each fragment, protected by apiezon wax remained unetched and served as a reference level).

The data, Table 11 and Figure 5, show that there is a flat Ti concentration profile in the as-grown wafer, with an average concentration of $\sim 7\times10^{13}$ cm^{-3}. However, in the cell fabricated from a similar as-grown wafer there is a steep profile. The Ti concentration near the junction is 1.76×10^{13} cm^{-3}; from there it increases then levels off to a value of $\sim 7\times10^{13}$ cm^{-3} at a distance of $\sim 10\mu m$ from the surface. Thus, following diffusion to form a solar cell, the majority of the bulk wafer ($\sim$ 250 μm) remains relatively unaffected, but the active center density within 10 μm of the surface diminishes substantially. About 70% of the solar radiation is absorbed in that first 10 μm thick region. Therefore, we expect a systematic increase in solar cell performance as the active center density (measured by DLTS) decreases, viz Table 10.

The concentration profile data at present are preliminary. Some further experiments are being conducted to substantiate the accuracy of the initial profile data.

3.2.2.2 Mo-doped Silicon

It is clear from Figure 4 that the effect of $POCl_3$ gettering on the relative cell efficiency (η/η_B) is small for Mo-doped silicon. A more careful look at the data, Table 12, reveals that the normalized cell efficiency increased only to 75% from an initial value of 72% even after the very intense gettering for 5 hours at 1100°C. This variation in the cell performance is small enough to result from process variations (the data represent the average efficiencies of 5-10 cells) or some inaccuracy in the measurements and data reduction. Therefore, we under-

TABLE I

Profile of the active Ti concentration in the starting wafer and solar cell each containing a metallurgical concentration of 2.1×10^{14} cm^{-3} Ti (Ingot W137Ti)

STARTING WAFER

DEPTH (μm)	ACTIVE Ti CONCENTRATION N_T (cm^{-3})
0	6.90×10^{13}
2.6	7.0×10^{13}
4.8	7.0×10^{13}
8.4	6.32×10^{13}
9.6	7.0×10^{13}

SOLAR CELL

0.4	1.76×10^{13}
2.2	3.19×10^{13}
4.4	6.6×10^{13}
6.0	7.18×10^{13}
10.0	7.6×10^{13}

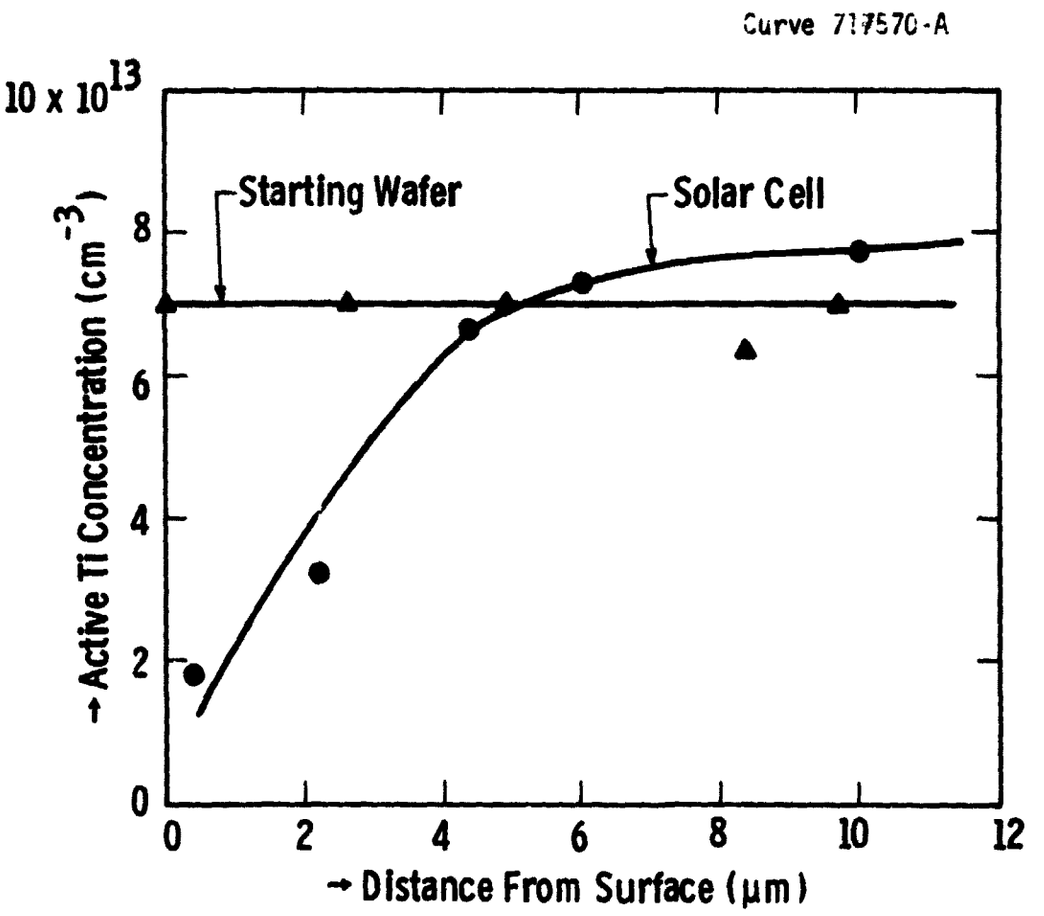

Figure 5 Depth Profile of Active Ti Concentration in an As-grown Wafer and Solar Cell Fabricated from a Silicon Ingot Containing a Concentration of 2.1×10^{14} cm^{-3} of Titanium

TABLE 12

Variation in cell efficiency and trap concentration (N_T) as a function of gettering treatment for Ingot 139 (original metallurgical Mo concentration $4.2 \times 10^{12} cm^{-3}$).

GETTERING CONDITION	NORMALIZED CELL EFFICIENCY (η/η_B), (%)	N_T (cm^{-3}) of E_V+0.30eV Trap
None- (Starting wafer)	-	4.45×10^{12}
None- (Solar Cell)	72.3	4.4×10^{12}
950°C/1 hr.	76.4	4.7×10^{12}
1000°C/1 hr.	72.2	4.5×10^{12}
1100°C/1 hr.	75.7	5.4×10^{12}
1100°C/2 hr.	66.7	2.2×10^{12}
1100°C/3 hr.	77.4	1.35×10^{12}
1100°C/5 hr.	75.3	1.0×10^{12}

took to examine in detail the gettering of Mo-doped ingot W139Mo by deep level transient spectroscopy.

To perform the analysis the front contact-grids were removed from the solar cells. Thirty mil diameter Ti-Au contacts then were deposited and mesas etched for the DLTS measurements. The DLTS results are listed in the right hand column of Table 12.

Mo exhibits one peak in the DLTS spectrum; analysis shows that the energy of this recombination center is E_V+0.3eV. The active Mo concentration both in the starting material and in the cells without any gettering is about $4.5x10^{12}cm^{-3}$. This value is nearly the same as the metallurgical concentration of Mo in the ingot, Table 12. This strongly suggests that all the Mo is electrically active in the as grown ingot and that the activity is little affected by the solar cell diffusion cycle.

When the gettering temperature is increased to 1100°C from 950°C no significant change is produced in the active Mo concentration. (The small scatter of the data from $4.5x10^{12}$ to $5.4x10^{12}cm^{-3}$ could be due to a slight variation in the impurity distribution. Similar results were found for ingot W138Mo. In that ingot the Mo concentration was about $1x10^{12}$ cm^{-3} and the active Mo concentration in the cell was ~ $1.5x10^{12}$ cm^{-3}.) However, when the gettering time was extended from 1 to 5 hours at 1100°C, we found a systematic reduction in active Mo concentration is observed, viz. Table 12. At the most intense gettering condition (1100°C/5hr) the electrically-active Mo concentration diminished to about $2x10^{12}cm^{-3}$, nearly a factor of 4 reduction from the ungettered value. Thus the slight increase in the cell efficiency is a real effect. (DLTS data on gettering of Ti at 1100°C for 5 hrs. showed about 2 orders of magnitude reduction in active Ti concentration compared to metallurgical Ti concentrations in the starting ingot).

This observation suggests that Mo is much more difficult to getter and thus may diffuse more slowly in silicon than does Ti. One result of this postulated behavior would be a steeper, narrower impurity

profile for Mo than for Ti during gettering. If this were so, it would explain why no significant performance improvement was detected even though the active Mo concentration near the junction was reduced four-fold. A series of experiments are being carried out to test this conjecture.

3.2.3 Detailed Analysis of HCℓ Impurity Gettering

As in the case of the $POCℓ_3$ experiments, Section 3.2.2, we have carried out a detailed analysis of HCℓ gettered specimens by DLTS. A preliminary analysis of the data, Table 13, shows that HCℓ gettering induced no systematic or significant improvements in the performance of Mo-doped solar cells, a result somewhat similar to our experience with the $POCℓ_3$ treatment. The DLTS data do show that the Mo concentration (near the junction) diminishes by about half after a 1000°C/1 hour treatment. Further increasing the gettering intensity had no appreciable effect in the trap density.

An explanation for the rather poor response of Mo to gettering treatments may lie in the way it diffuses in the silicon lattice. If Mo diffuses slowly in silicon as we suspect then a very narrow Mo depletion profile (<< 10 μm) may be formed during gettering in contrast to the wider profile in the Ti-doped material, viz. Figure 5. This being so, the reduction in Mo content measured by DLTS would lie very close to the junction and affect only a very small portion of the carriers in the wafer. The cell performance would show little improvement in this case.

The main difference between the $POCℓ_3$ (Table 12) and HCℓ (Table 13) data appears to be the ability of the HCℓ treatment to reduce the active Mo concentration even after the 1000°C processing while temperatures of 1100°C are required before $POCℓ_3$ produces a measureable reduction in the center density. This difference may stem from the fact that the $POCℓ_3$ gettering produces a junction which is subsequently etched off before the solar cell fabrication is carried out. As much as 12.5 μm of silicon may be removed after $POCℓ_3$ gettering while only about 0.1 μm of silicon is etched away to remove the oxide formed by HCℓ gettering. Following our postulation of the narrow Mo profile, then we might expect that variations in the amount of gettered material removed could indue some variability into the cell performance data.

TABLE 13

Variation in Trap Center Density and Relative Cell Efficiency as a Function of HCℓ Gettering Treatment for Mo-doped Silicon (Ingot W-139-Mo) and Ti-doped Silicon (Ingot W-137-Ti).

INGOT W139 MO

Gettering Condition	$N_T(cm^{-3})$	$\eta/\eta_B(\%)$
None (cell)	4.4×10^{12}	72.3
1000°C/1 hr.	1.9×10^{12}	63.7
1100°C/1 hr.	1.9×10^{12}	70.0
1100°C/5 hr.	2.2×10^{12}	66.0

INGOT W137 TI

Gettering Condition	$N_T(cm^{-3})$	$\eta/\eta_B(\%)$
None (cell)	1.76×10^{13}	42.8
1000°C/1 hr.	-	68.8
1100°C/1 hr.	-	73.1
1100°C/4 hr.	-	68.2

For Ti, HCℓ gettering raises the relative cell efficiency to 68.8% of baseline after 1 hour at 1000°C compared with 42.8% for the ungettered cell, Table 13. We could detect no electrically active Ti near the junctions in these cells. $POCℓ_3$ gettering for the same time and temperature raised normalized cell efficiency to only 51%. An active Ti concentration of 3.94×10^{12} cm^{-3} was measured, Section 3.2.2.

The difference in behavior again may be ascribed to the etching subsequent to the HCℓ and $POCℓ_3$ treatments. If a significant amount of the silicon in which the Ti concentration had been reduced was removed by etching after the $POCℓ_3$ treatment we might expect to observe a lower cell efficiency compared to the HCℓ-gettered cells (again recall that about 70% of the solar radiation is absorbed in the first ten or so microns of the device).

We plan to evaluate these ideas in some future experiments.

3.2.4. Model Analyses of Gettering Behavior in Silicon

The results of the gettering experiments described in the foregoing sections indicate significant cell performance increases for Ti or Fe-doped silicon after gettering and considerably less change for Mo-doped material. Questions arise as to (1) how these results correlate with previous impurity-cell performance data[1,2] and (2) how realistic is our picture of the gettering as a diffusion dominated process. These two topics are considered below.

3.2.4.1 Application of Cell Performance Model to Gettered Devices

We assume that gettered samples differ from the ungettered ones only in terms of the degree of electrical activity of the impurity. It is then possible to use the impurity model[1,2] to obtain a relationship between cell performance and the change in impurity activity. For the ungettered device:

$$\left(\frac{I_{n\infty}}{I_{n1}} - 1\right)^2 = C_1 + C_{2x} N_x \qquad (1)$$

where C_1 and C_{2x} are constants defined as described in Reference 1 and N_x is the metallurgical impurity concentration in the silicon. And for the gettered device:

$$\left(\frac{I_{n\infty}}{I_{n2}} - 1\right)^2 = C_1 + K_a C_{2x} N_x \qquad (2)$$

where K_a is the relative change in active impurity centers. Solving (1) and (2) for K_a:

$$K_a = \frac{\left(\frac{I_{n\infty}}{I_{n2}} - 1\right)^2 - C_1}{\left(\frac{I_{n\infty}}{I_{n1}} - 1\right)^2 - C_1} \qquad (3)$$

K_a can be determined experimentally from the DLTS trap density measurements or calculated directly from Eq. (3) using the measured values of I_{n1} and I_{n2} obtained from the solar cells. A comparison of calculated and measured results for Ti and Mo-doped ingots is shown in Table 14.

The data for the two titanium doped ingots are well behaved but the values for N_T and K_a calculated from the measured short circuit currents are larger than those measured by DLTS. This implies that the total effective titanium trap density in the solar cells is larger than is present in the junction depletion region where the deep level measurement is made. This is consistent with the idea that the gettering of titanium is limited by its ability to diffuse to the phosphorus-rich surface region, and this results in a titanium concentration which is smaller near the surface and junction than in the interior of the base region. Further experiments like those described in section 3.2.2 to examine this profile will permit accurate calculation of the effective trap density and cell performance effects produced by the gettering processes.

TABLE 14

COMPARISON OF CALCULATED AND MEASURED GETTERING DATA

INGOT W137 Ti (2.1×10^{14})

Hering Process Temp. (°C)	Time (H)	I_n	η_n	Measured $N_T(10^{12})$	K_a	Calculcated $N_T(10^{12})$	K_a
None		.565	.428	17.6	1	(17.6)	1
950	1	.588	.467	6.35	.361	14.87	.845
1000	1	.638	.510	3.94	.224	10.26	.583
1100	1	.653	.529	2.99	.170	9.16	.520
1100	2	.674	.554	2.50	.142	7.79	.443
1100	3	.692	.591	3.39	.193	6.76	.384
1100	5	.713	.662	1.49	.085	5.71	.324

INGOT W134 Ti (3×10^{13})

None		.689	.579	3.60	1	(3.60)	1
950	1	.721	.590	2.27	.631	2.78	.722
1100	1	.735	.615	1.65	.458	2.47	.687
1100	3	.787	.705	0.50	.139	1.56	.435
1100	5	.818	.769	<.25	<.069	1.15	.319

INGOT W139 Mo (5.4×10^{12})

None		.835	.723	4.43(?)	1	(4.43)	1
950	1	.843	.764	6.00	1.354	4.06	.916
1000	1	.845	.722	4.50	1.016	3.97	.895
1100	1	.858	.757	5.40	1.219	3.41	.770
1100	2	.801	.667	2.20(?)	.497	6.28	1.418
1100	3	.877	.774	1.35	.305	2.69	.607
1100	5	.864	.753	.900	.203	3.17	.716

The data for molybdenum, Table 14, are less well behaved and show considerable scatter. It is apparent however, that molybdenum is not as readily gettered as is titanium, a point already noted in earlier discussions. The data also show the same general relationship between the calculated and measured numbers, i.e the effective trap density in the cell is larger than implied by the deep level concentration measurements. We conclude,therefore,that the gettering of molybdenum is also diffusion-limited and furthermore, molybdenum either has a much smaller diffusion constant than titanium,or phosphorus is unable to complex and deactivate molybdenum as readily as titanium.

3.2.4.2 Diffusion of Ti during $POCl_3$ Gettering

The gettering process can be examined mathematically as a diffusion process by assuming that at the phosphorus-rich surface region of the wafer the metallic impurity is forced to a fixed concentration. Before the gettering process the wafer is assumed to have a uniform initial impurity concentration throughout its thickness. The one-dimensional diffusion equation is given by:

$$\frac{\partial N(x,t)}{\partial t} = D \frac{\partial 2N(x,t)}{\partial x^2} \tag{4}$$

where N(x,t) is the impurity concentration as a function of distance from the center of the wafer and the time of the gettering process. D is the diffusion constant for the impurity in silicon. The general solution of (4) can be expressed as:

$$N(x,t) = (A \sin\alpha x + B \cos \alpha x) \exp(-\alpha^2 Dt) \tag{5}$$

The boundary conditions,

$$N\left(-\frac{W}{2},0\right) = N\left(\frac{W}{2},0\right) = N_s \tag{6}$$

$$\text{and } N(x, 0) = N_o, \tag{7}$$

provide a solution in series form:

$$N(x,t) = N_s + \frac{4}{\pi}(N_o - N_s) \sum_{j=o}^{\infty} \frac{(-1)^j}{2j+1} \cos \frac{(2j+1)\pi x}{W} \exp\left[\left[\frac{(2j+1)\pi}{W}\right]^2 Dt\right] \quad (8)$$

where W is the sample thickness, and N_o and N_s are the initial and surface impurity concentrations.

While this solution is suitable for fast diffusing impurities, the series converges very slowly for slowly diffusing species or short times. In this latter case a mathematically equivalent solution may be obtained which converges more rapidly.

$$N(x,t) = N_o - (N_o - N_s) \left[\sum_{j=o}^{\infty} (-1)^j \operatorname{erfc} \frac{(2j+1)\frac{W}{2} - x}{2\sqrt{Dt}} + \sum_{j=o}^{\infty} (-1)^j \operatorname{erfc} \frac{(2j+1)\frac{W}{2} + x}{2\sqrt{Dt}} \right] \quad (9)$$

Phosphorus gettering of titanium was examined experimentally using DLTS measurement on step-etched surfaces to obtain the concentration profile. These data shown in Figure 5 suggest values for $N_o \cong 8\text{x}10^{13}/\text{cm}^3$ and $N_s \cong 8\text{x}10^{12}/\text{cm}^3$. It is assumed the gettering surface, where N_s is applicable, is located at the n-p junction. The gettering process for this sample consisted of an 850°C, 1 hour phosphorus diffusion.

Fitting the series solution given in (9) to these data, Figure 6, implies a diffusivity for titanium, $D \cong 1.27\text{x}10^{-11}$ cm^2/sec (at 850°C). This result is about 3 times larger than the value extrapolated from the data of reference 5 which was obtained by Ti in-diffusion at temperatures between 1000°C to 1250°C. Although based on a single experiment the agreement is close enough to give the model credibility. Moreover, limited data from more intensively gettered samples are also in nominal agreement with this result.

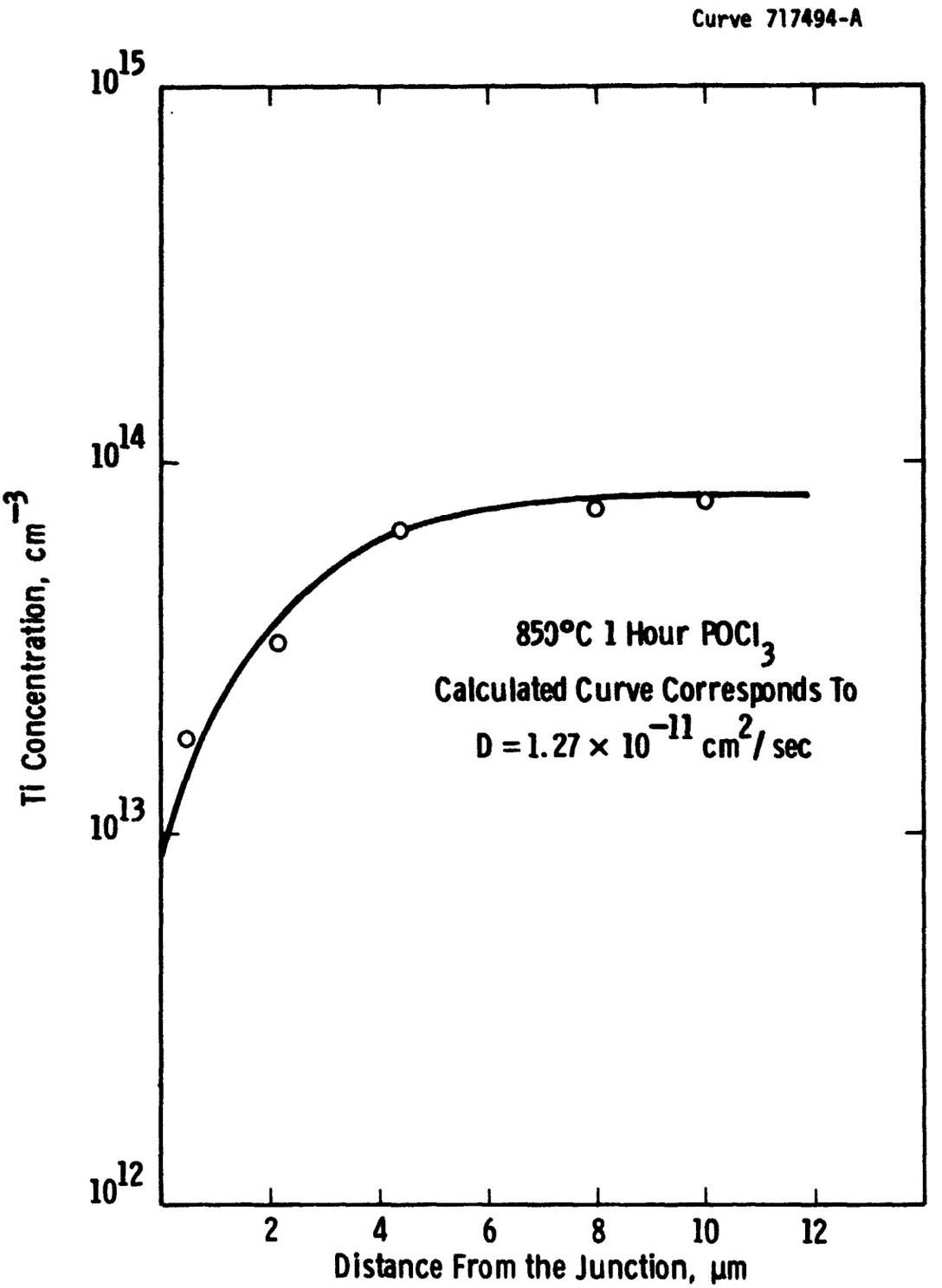

Figure 6 Calculated Ti Diffusion Profile in a Silicon Wafer Following Gettering in $POCl_3$ at 850°C

Besides providing a credible mechanism for the gettering results, the model coupled with the impurity profile data provides an interesting method for obtaining diffusion constants.

Some additional comments are warranted with regard to the model. The titanium concentration data used for the analysis were the electrically active concentrations observed by the DLTS measurements, and we have assumed a constant ratio of electrically-active center density to the metallurgical density; (this assumption is supported by DLTS data obtained from samples doped with various metallurgical Ti concentrations). Given a constant ratio of electrically active centers the linearity of the diffusion equation allows us to use either DLTS concentrations or metallurgical values and obtain the same result.

Impurities in a crystal lattice may occupy a number of non-equivalent positions, for example substitutional or interstitial. Such nonequivalent sites should be expected to have distinctly different bond relationships with the host lattice and thus correspondingly different electrical activities. This mechanism in addition to precipitation or aggregation provides a basis for the observed difference between electrical activity and impurity concentrations.

In a similar way, the diffusion of impurities in a crystal is subject to site dependencies and, therefore, will display variation as a function of which mechanism is dominant. These considerations suggest that for some impurities we may expect non-linear influences on the gettering process due to temperature and complexing behavior. Experiments are in progress to examine these phenomena which may provide a basis for describing an optimum gettering procedure.

3.3 The Synergic Interaction of Cu with Other Transition Elements

In Reference 1 we showed that the cell performance of silicon devices contaminated with Ti or V could be improved somewhat by the addition of greater than 10^{15} cm^{-3} Cu as a co-dopant. Since that time we have utilized DLTS measurements to investigate this synergic behavior in more detail. The initial results can be understood with the aid of the data

in Table 15. In the Table are listed the metallurgical impurity concentration (N_M), the electrically active impurity concentrations in the as-grown ingot (N_S) and cells made therefrom (N_C), the ratios N_S/N_M and N_C/N_M, and finally the normalized cell efficiency for ingots containing Ti, V, or Mo and the same impurities plus a Cu addition.

From the data it is evident that only about one third of the total metallurgical titanium added to the ingot is active. The addition of $2x10^{15}$ cm^{-3} of Cu reduces this active fraction in the as-grown material to 0.26. (based on the E_V+0.3eV trap). A similar decrease in the active Ti ratio (N_C/N_M) in the cell to 0.04 from 0.08 when Cu is added accounts for the improvement in relative cell efficiency to 48% of baseline compared to 42% when Cu is absent. (The absolute values of impurity concentrations may not apply to the bulk wafer due to the concentration profile formed during cell diffusion, Section 3.2.2)

In the case of vanadium only about 0.087 of the metallurgically-added element remains electrically active in the as-grown ingot. When Cu is added at a concentration of about $2x10^{15}cm^{-3}$, the active vanadium fraction diminishes to 0.073, again illustrating a small but observable synergic effect (here the activity refers to the concentration of E_V+0.42eV traps). As yet we have no data for the activity ratio of vanadium in the cells, information which is necessary to explain the rather large improvement in cell efficiency-38 to 57% of baseline-accompanying the Cu additions.

Nearly all of the Mo added to the ingot is electrically active in the as-grown wafers (and in the solar cells as well). Adding Cu to the Mo-doped material produces no significant change in the concentration of electrically active Mo species or in the cell performance. We conclude that unlike Ti or V no synergic reaction between Mo and Cu occurs.

TABLE 15

The Effect of Copper on the Relationships Between Solar Cell Performance and the Electrically Active Impurity Concentration in Silicon

Ingot ID	Metallurgical Concentration N_M cm^{-3}	Active Concentration in the as-grown matl. N_S cm^{-3}	Active Concentration in the cell N_C cm^{-3}	$\frac{N_S}{N_M}$	$\frac{N_C}{N_M}$	η/η_B(%)
W137Ti	2.1×10^{14}	7.0×10^{13}	1.76×10^{13}	.33	.084	42.0
W104Ti/Cu	$(1.4/20) \times 10^{14}$	3.6×10^{13}	6.11×10^{12}	.26	.04	48.0
W009V	4×10^{14}	3.5×10^{13}	-	.087	-	38.0
W111V/Cu	$(3/2.5) \times 10^{14}$	2.2×10^{13}	-	.073	-	57.0
WMo077	4.2×10^{12}	4.16×10^{12}	3.95×10^{12}	.99	.95	74.0
W141Mo/Cu	$(4.0/4000) \times 10^{12}$	-	4.4×10^{12}	1.1	-	72.0

3.4 Investigations of Anisotropic Impurity Distributions in Silicon

Recent effort on this task has primarily been to prepare impurity-doped material for subsequent assessment of any deleterious effects on cell performance due to non-uniform impurity distribution. Two types of crystals have been produced, 7.6cm diameter Czochralski ingots, to study impurity behavior in silicon produced by conventional growth processes[3] and 3 to 4 cm wide silicon webs[6] on which we plan to evaluate impurity effects in ribbon-type silicon.

Previously we showed that Ti and Mn, impurities which diminish cell performance by reducing bulk lifetime,[1] produced no excess performance degradation on large diameter wafers that could be ascribed to non-uniform impurity distribution.[3] We have now grown two more large diameter Czochralski ingots doped, respectively, with 2.4×10^{16} Cu and 5.1×10^{14} Fe. Cu degrades cell performance primarily by junction mechanisms while Fe affects the junction as well as bulk lifetime. Wafers from these two ingots, W-172 and W-173 are now under evaluation, and should provide us with data on any contrasts in behavior due to the different degradation mechanisms involved.

We have also prepared silicon web crystals doped with Ti and V at target levels of about 1.2 and 1.5×10^{13} cm^{-3}, respectively. The variation in cell performance and electrical properties across the ribbons (which are 3 to 4 cm wide) will be examined via miniature solar cells and deep level transient spectroscopy. Any variation in the properties of the ribbons associated with transverse variations in impurity concentration should be evident.

3.5 The Permanence of Impurity Effects in Silicon Solar Cells

To determine the stability of cell characteristics under long term operating conditions, we are carrying out a series of high temperature heat treatments on both contacted and uncontacted wafers. Following thermal stressing the wafers are contacted where required and the solar cell parameters are determined. By proper modeling of these high temperature effects it should be possible to approximate the time to failure for the impurity-doped solar cell operating under realistic conditions.

The experimental procedure has been described earlier[3], but briefly, selected wafers are annealed under differing thermal stresses and the cell results compared to baseline wafers treated in the same way.

Most of the data gathered thus far have been measured on ingots doped with Ti and Mo:

$$W123Ti\text{-}008\ (1x10^{14}Ti/cm^3)$$

$$W077Mo\text{-}001\ (4.2x10^{12}Mo/cm^3)$$

In addition, initial data on ingot W072Cr005 ($2.8x10^{14}Cr/cm^3$) is given in this report. The baseline ingot W097-00-000 has been processed concurrently with the impurity-doped material in all tests.

Our initial studies indicated that the contacted solar cells failed after a short period of time at 500°C. Dark I-V data indicated junction degradation which we assume is due to the diffusion of the contact metals (Ti-Pd-Ag) into the junction. Since the main thrust of the investigation now is to evaluate long term effects due to the electrically-active dopant or metal contaminant in the bulk material, all high temperature experiments have been carried out on diffused but uncontacted wafers.

We reported data for aging experiments on Mo and Ti ingots up to 800°C in the last report.[3] The Ti ingot exhibited essentially no change in properties after 100 hrs at 800°C, while the cell performance of the Mo ingot dropped to about 0.95 of its unannealed value;(the baseline ingot degraded to 0.8 of its unannealed value after this same treatment).

Further aging tests have now been carried out on the Mo and Ti ingots. In these tests,the wafers were annealed at 900°C for 1, 10, and 100 hours, Table 16. As in the 800°C cases, the Ti-doped ingot shows little change in efficiency after 100 hrs at 900°C (4.94%-4.65%). The efficiency of both the Mo and baseline cells decreased by more than

TABLE 16

AGING OF TI AND MO-DOPED SILICON AT 900°C

W097 Baseline
W077 Mo
W123 Ti

	I_{sc}	V_{oc}	FF	η	τ_{OCD}	η/η_o
As Fabricated						
W-097	21.20	.554	.738	9.16	4.6	1.0
W077	18.80	.515	.703	7.18	.9	1.0
W123	13.95	.485	.691	4.94	.8	1.0
1 HR - 900°C						
W097	20.25	.546	.742	8.67	2.5	.95
W077	17.90	.504	.700	6.68	.5	.93
W123	13.80	.489	.706	5.04	.7	1.0
10 HRS 900°C						
W097	15.40	.502	.677	5.53	.7	.60
W077	10.30	.434	.685	3.24	.9	.45
W123	13.60	.488	.690	4.87	.6	.99
100 HRS 900°C						
W097	9.9	.446	.703	3.25	.7	.35
W077	9.50	.418	.664	2.79	.5	.39
W123	13.10	.483	.697	4.65	.6	.94

one half of their unannealed value. The last column (η/η_o) in Table 16 is the ratio of the efficiency after annealing to the unannealed value.

If we define time to failure as the time, at a given temperature, for which the efficiency decreases to 90% of the unannealed value, it is possible to extrapolate the 800°C and the 900°C data to determine the time dependence at any lower temperature. The data for this calculation are given in Table 17. We estimate that the numbers in Table 17 are accurate to $\pm$ 50%.

Plotting the data in Table 17 in an Arrhenius form allows us to estimate the time to failure near the typical maximum operating temperature of a deployed solar array. This extrapolation is illustrated in Figure 7 for both the baseline and Mo-doped specimens. Clearly, extrapolation from such limited data over several orders of magnitude can give misleading results. However, assuming the worst possible error as a first order approximation, this extrapolation gives a time to failure at 200°C as > 10^5 hrs (20 years: 1.75×10^5 hours). The precision of the extrapolation will be improved as more data are collected.

A Cr-doped ingot (W072Cr005-2.8×10^{14} Cr/cm^3) has recently been added to the study. In view of the relatively small effects exhibited by Ti and Mo at lower annealing temperatures the tests on the Cr-doped material were begun at 800°C. Since Cr is a fast diffuser in Si, data for 800°C, 600°C, and 500°C should suffice to derive a time to failure.

In Table 18 are listed the 800°C annealing data for the Cr-doped ingot; baseline data are included for comparison. With the same definition for time to failure noted above the Cr ingot falls to 90% of its initial value in 2 hours at 800°C. These experiments will continue in succeeding months.

3.6 The Effect of Construction Material Contaminants on p-base Solar Cell

We showed in Reference 1 that, for the majority of impurities, the mechanism of performance reduction in silicon solar cells was the impairment of bulk lifetime by the formation of carrier recombination

TABLE 17

TIME TO FAILURE (90% OF UNANNEALED PERFORMANCE)
FOR BASELINE AND METAL-DOPED INGOTS

800°C

INGOT	HRS TO FAILURE (± 50%)
W097 BASE	50
W077 Mo	100
W123 Ti	300

900°C

W097 BASE	1.5
W077 Mo	1.5
W123 Ti	300

HRS TO FAILURE = Time at given temperature at which cell efficiency decreases to 90% of unannealed value

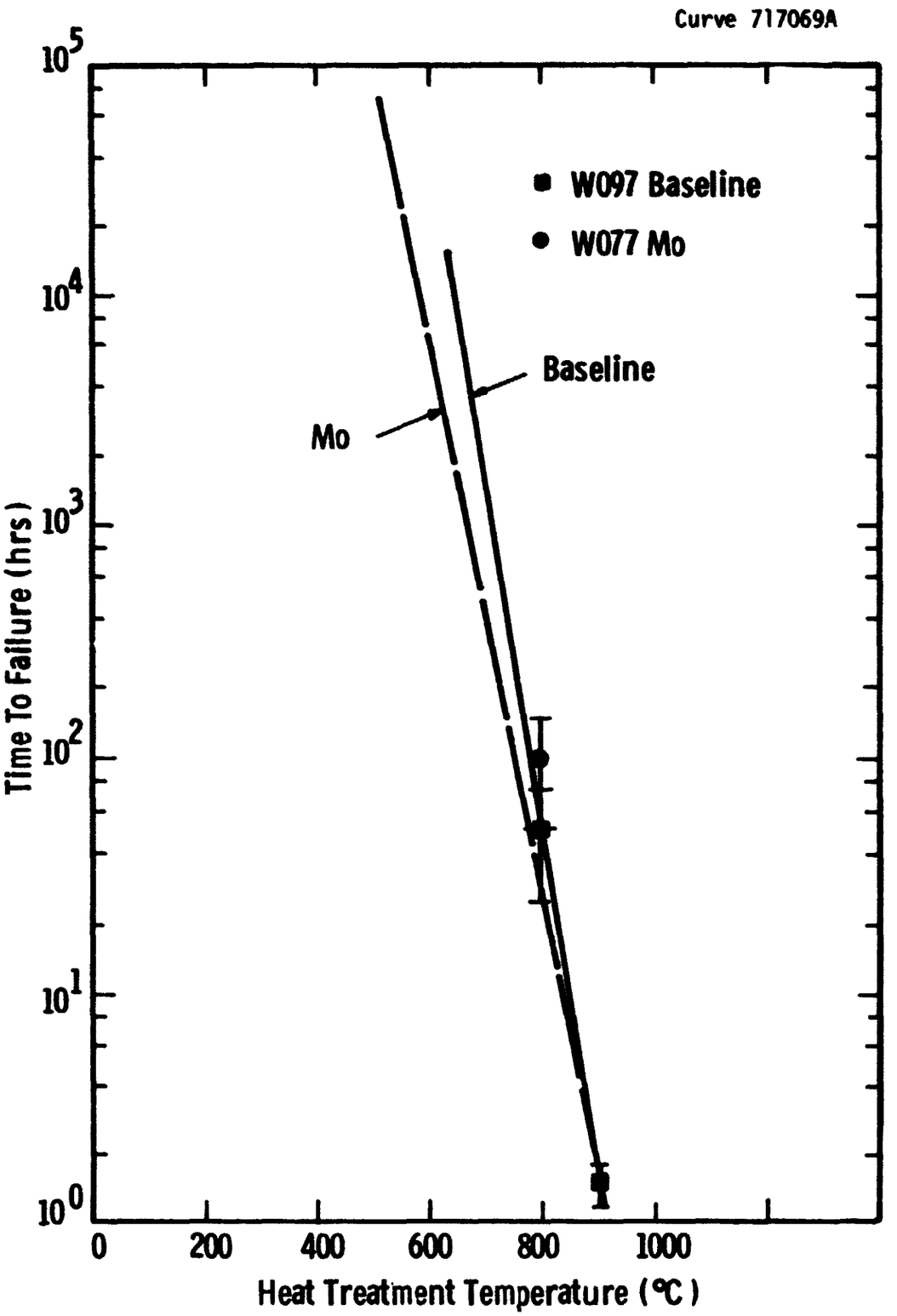

Figure 7 Time to Failure (90% of unnnealed cell performance) for Baseline and Mo-doped Silicon

TABLE 18

AGING OF Cr-DOPED SILICON AT 800°C

W072CR005

W09700000

	I_{sc}	V_{oc}	FF	η	τ_{OCD}	η/η_o
As Fabricated						
W097	22.20	.577	.727	9.85	5.0	1.0
W072 Cr	20.43	.542	.746	8.73	2.3	1.0
1 HR @ 800°C						
W097	22.00	.551	.739	9.40	5.0	.95
W072 Cr	20.04	.534	.731	8.23	1.6	.94
10 HR @ 800°C						
W097	21.35	.545	.744	9.20	6.5	.92
W072 Cr	18.55	.521	.713	7.29	.9	.84
100 HRS @ 800°C						
W097	18.80	.553	.743	7.85	3.0	.82
W072 Cr	13.93	.476	.679	4.76	.9	.55

centers. This result led us to formulate an impurity-performance model relating cell efficiency to the amounts of single, or multiple metal species present in the silicon The original data, based primarily on impurities present in the raw materials from which poly-crystalline silicon is made, has now been augmented with information on contaminants likely to be introduced during subsequent processing of the silicon. These impurities include W, Ta, Mo, Nb and Co, commonly employed as refractory components in high temperature process equipment such as crystal growth furnaces.

Figure 8 depicts the variation in cell performance with impurity concentration for the refractory metals as well as for impurities previously studied.[1,2] The curves are derived fitting the impurity effects model to the cell performance and impurity concentration data. For Mo and Ta, the curves have been revised from earlier results to reflect an increase in the number of ingots studied and improvements in the segregation coefficient data (see section 3.1.1). The projected curves for W, Nb, and Co are based on at most three data points and must be considered preliminary at this time.

One remarkable aspect of the relationships plotted in Figure 8 is the general regularity of impurity behavior with position in the Periodic Table. Elements located to the right in the transition metal row, Cu and Ni, have the least impact on performance. As one moves to the left the severity of performance degradation increases being modest for Co, Fe, Mn and Cr and severe for Ti and V. Within a column of the Table performance degradation increases with atomic number; for example, Ta is worse than Nb which is in turn worse than V . Since the impurity segregation coefficients for crystal growth (Table 1) generally are smallest for the most harmful impurities, nature has, in a sense, mitigated the situation.

3.7 Degradation of N-base Solar Cells by Impurities

3.7.1 Single Impurity Behavior

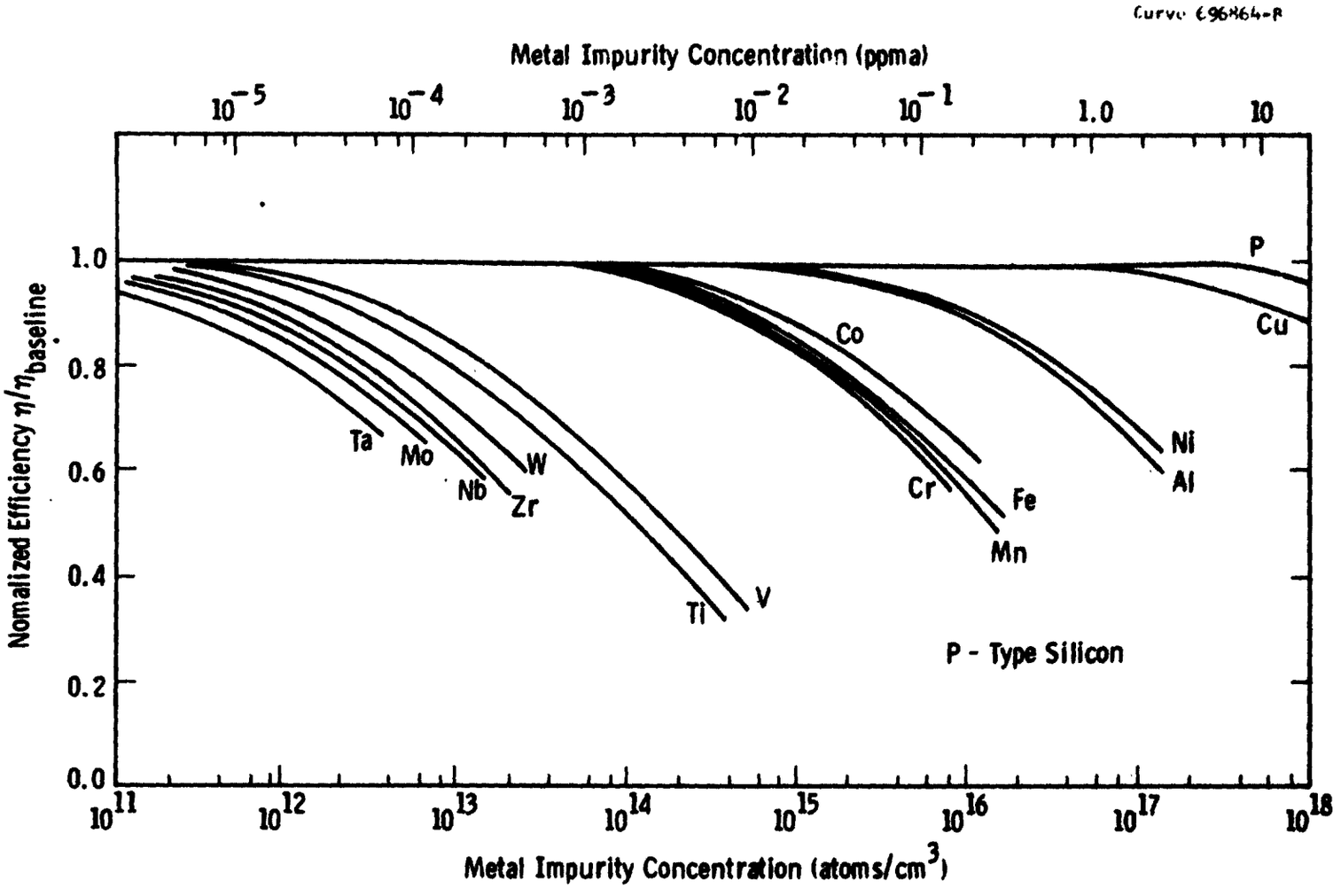

Figure 8 Model-derived Impurity-Performance Curves for Single Metal Contaminants in p-type Silicon. The Curves for Mo, Ta, W, and Co are Calculated From Recent Cell Efficiency and Impurity Concentration Data; Relationships for the Other Impurities are from Reference 1.

We have augmented the previous results on n-type silicon with information from second and third generation ingots (W147 to 150 and W153 to 156) doped with Ni, Mn, Fe, V, Ti, Cr and Mo as well as the first multiply-doped n-type ingots (W157 to 159 and W177 and 178). The revised impurity-performance curves, Figure 9, for single impurities confirm the general conclusions developed earlier.[1]

As for p-base devices, the observed cell performance degradation can be modeled on the basis of a reduction in bulk lifetime due to the formation of recombination centers by the contaminants. The data for Ni-connected by a dashed line in the figure -- are the most notable exception. These points cannot be fitted to our model since junction degradation mechanisms, rather than lifetime reduction, are the dominant mode for the decrease in cell efficiency.

We pointed out before that for many impurities device performance seemed to be less effected in the n-base cells than in comparable p-base cells.[1] This behavior can be visualized with the aid of Figure 10. In the figure we plot the threshold impurity concentrations (N_{ox}) for which cell performance reduction initiates in each of the two types of devices. Points falling on the 45° line in the graph are for impurities behaving identically in n and p-base cells, points above the line indicate impurities which produce less degradation in n than in p-base cells. The majority fall in the latter catagory, Cr and Fe being in the former. Only Cu and Ni (not illustrated) degrade the n-devices more severely, apparently by junction mechanisms.

3.7.2 Effects Due to Multiple Contaminants

By means of the model coefficients used to derive the curves in Figure 9, we can also project the expected performance of solar cells doped with multiple contaminants.[1] Table 19 lists the impurity concentrations in the multiply-doped n-base ingots we have studied so far. A comparison of the projected and measured cell performance data for the ingots is given in Table 20. Generally, the data show fair agreement between the expected and observed values.

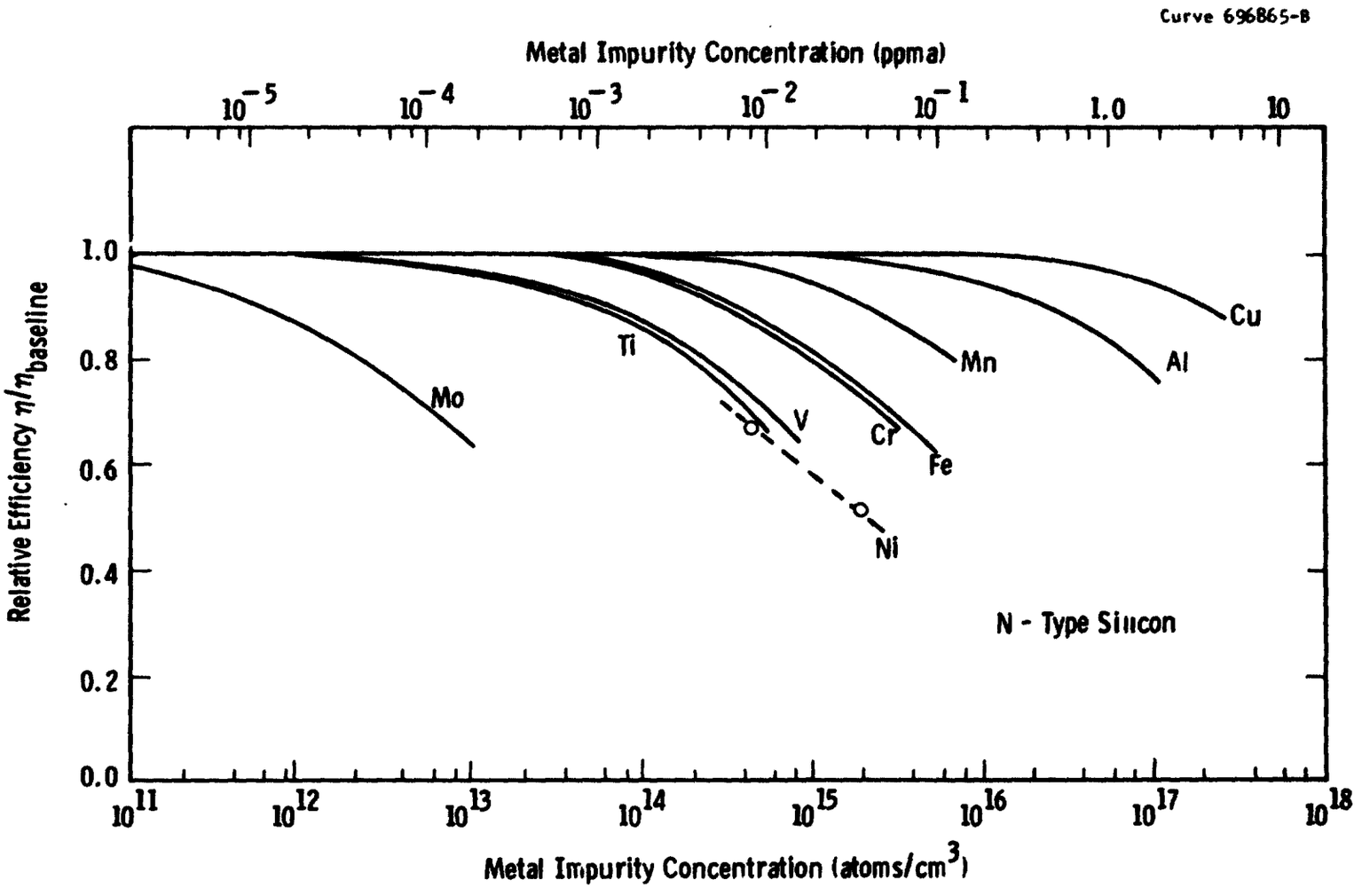

Figure 9 Model-Derived Impurity-Cell Performance Curves for Single Impurities in N-type Silicon.

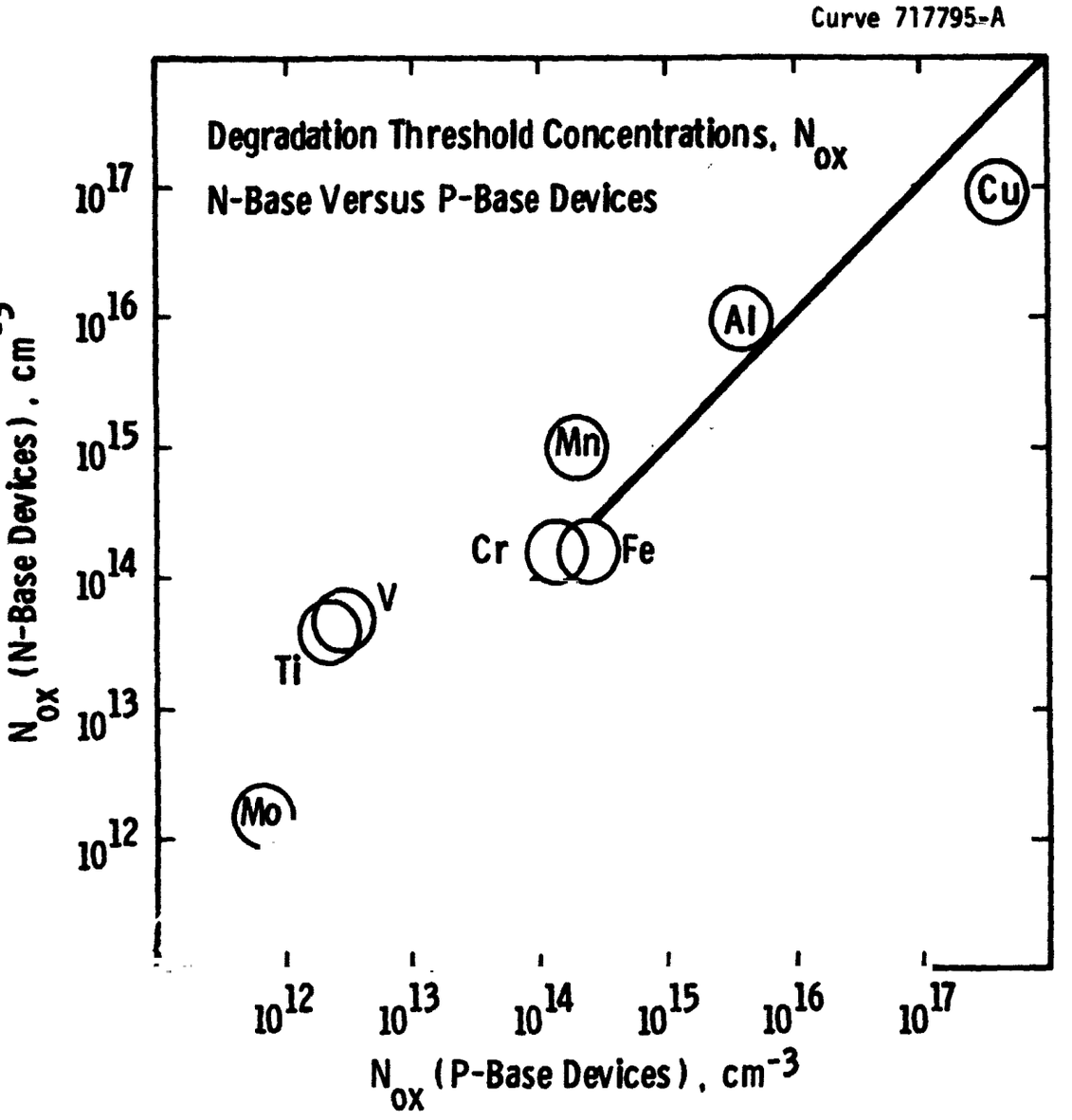

Figure 10 Comparison of Impurity Behavior in N and P-Base Solar Cells

TABLE 19

IMPURITY CONCENTRATION OF MULTIPLY-DOPED N-BASE INGOTS

	Impurity Concentration (cm^{-3})			
Ingot	Ti	V	Cr	Mn
W157	$8x10^{13}$	$1.2x10^{14}$	-	-
W158	$5x10^{13}$	$5x10^{13}$	$5.5x10^{14}$	-
W159	$2x10^{13}$	$2x10^{13}$	$3.5x10^{14}$	$3.2x10^{14}$
W176	-	-	$1.2x10^{15}$	$1.26x10^{15}$
W178	$8x10^{13}$	-	-	$8.6x10^{14}$

TABLE 20

COMPARISON OF MEASURED AND CALCULATED CELL PERFORMANCE
FOR MULTIPLY-DOPED N-BASE INGOTS

Ingot	I_{sc}/I_{sco}x100		n/n_ox100	
	Measured	Calculated*	Measured	Calculated*
157-Ti/V	82.5± 1.9	86.0±8.4	77.1±5.0	81.0±11.0
158-Cr/Ti/V	88.1±1.4	84.9±9.1	80.4±5.6	79.2±11.8
159-Cr/Mn/Ti/V	88.3±1.3	90.2±6.4	74.6±12.7	85.9±8.8
177-Cr/Mn	84.7±5.0	81.4±10.7	78.6±7.4	75±13.4
178-Mn/Ti	No cell data available			

*See section 4.3 and 4.4 of Reference 1.

4. CONCLUSIONS

The segregation coefficients of W, Ta, and Co determined from neutron activation analysis data are very small for Czochralski silicon crystal growth: $k_W = 1.7 \times 10^{-8}$, $k_{Ta} = 2.1 \times 10^{-8}$ and $k_{Co} = 1.0 \times 10^{-5}$. The values are consistent with those for other nearby elements in the Periodic Table, e.g. $k_{Mo} = 4.5 \times 10^{-8}$ is very close to the values for Ta and W while $k_{Ni} = 3.2 \times 10^{-5}$ is similar to the Co value.

The gettering of Ti, Mo and Fe by high temperature $POCl_3$ and HCl treatments is a diffusion-controlled process in which the impurities move outward from the bulk wafer to the phosphorus-(or chloride) rich surface of the material. Deep level spectroscopic measurements of the Ti recombination center density in $POCl_3$-gettered wafers show a concentration gradient in which the trap density is lowest near the surface then recovers to the (pre-diffusion) bulk value within 10 to 12μm into the wafer. The concentration profile can be fit by a mathematical function assuming Ti out-diffusion; the value of the Ti diffusion constant calculated this way is about 1.27×10^{-11} cm^2/sec, a magnitude consistent with published diffusion data. Mo, in contrast to Ti, appears to diffuse much more slowly in silicon so that gettering treatments are less effective for improving cell efficiency in this case.

We have derived impurity-performance curves for Mo, Ta, W, Nb, and Co on the basis of the most recent impurity and cell data, while the computations are somewhat preliminary, the data confirm trends observed earlier for other impurities: (1) elements farthest to the right in a row of the periodic table have less impact on cell performance than those to the left, e.g. Cu is relatively benign while Ti severely degrades performance; (2) within a column of the periodic table performance degradation increases from upper to lower position, e.g. V is less-harmful than Nb which is in turn less harmful than Ta; (3) elements which degrade

cell performance more have smaller segregation coefficients for crystal growth. Of the elements we have studied Ta has the lowest threshold for the onset of cell performance degradation, and one of the smallest k_{eff} values.

Impurity-performance curves for n-base cells, updated with second and third generation ingot data, illustrate that most impurities are less harmful to n than p-base cells. For example, Mo, Mn, Al, Ti, and V fall in this catagory. Fe and Cr behave about the same in both kinds of cells while Cu and Ni produce slightly greater degradation (by junction mechanisms) in the n than in the p-base devices.

5. PROGRAM STATUS

The program is on schedule as indicated by the current milestone chart, Figure 11.

5.1 Present Status

During the past report period we:

- prepared sixteen Czochralski ingots doped with various metal contaminants for subsequent chemical, microstructural, electrical and solar cell evaluation.
- completed the mass spectroscopic analysis of all ingots grown as well as sensitive neutron activation analysis of selected ingots.
- made the first reported measurements of the segregation coefficients of tungsten and tantalum in silicon.
- completed HCℓ gettering experiments on Fe, Mo, and Ti-doped silicon.
- extended $POCℓ_3$ gettering temperature range to 1200°C.
- performed a detailed assessment by deep level spectroscopy of Ti and Mo gettering by $POCℓ_3$ and HCℓ.
- mapped the profile of Ti impurity distribution following $POCℓ_3$ gettering.
- extended aging studies of impurity effects in silicon to 900°C.
- prepared silicon webs doped with Ti and V for anisotropy investigations.
- modeled the behavior of construction material impurities and metal impurities in n-base silicon.

PROGRAM PLAN (SCHEDULE)
(PHASE III)

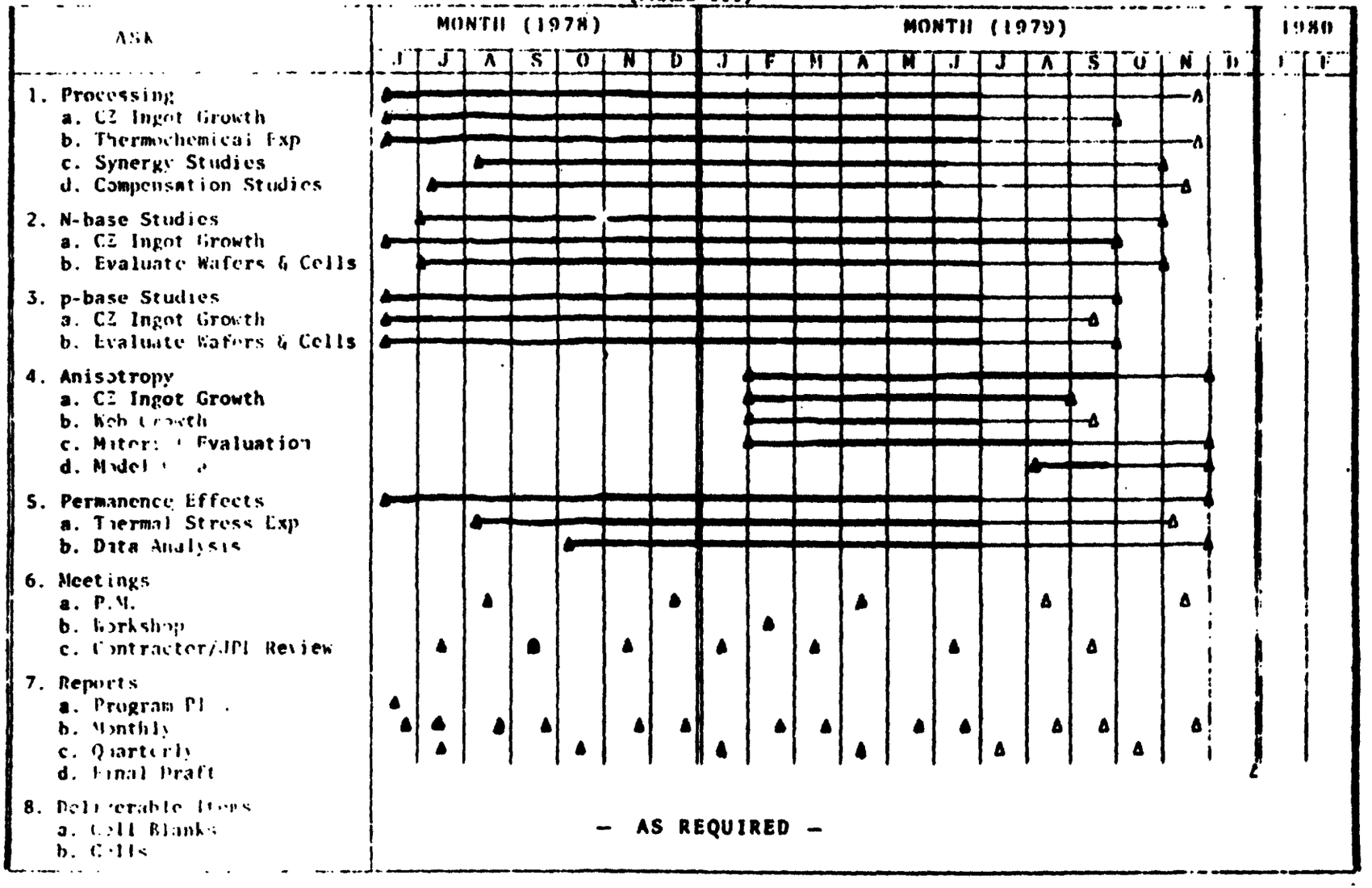

5.2 Future Activity

During the next quarter the majority of the experimental work on construction materials, anisotropy effects, n-base impurity effects and gettering of Ti, Mo, and Fe will be completed.

6. REFERENCES

1. R. H. Hopkins, et al., 11th Quarterly Report and Summary, Silicon Materials Task (Part 2) DOE/JPL 954331-78/3, July (1978).
2. R. H. Hopkins, et al., 5th Quarterly Report and Summary, Silicon Materials Task (Part 2) DOE/JPL 954331-77/1, January (1977).
3. R. H. Hopkins, et al., 14th Quarterly Report, Silicon Materials Task (Part 2) DOE/JPL-954331-79/2 April (1979).
4. R. H. Hopkins, et al., 3rd Quarterly Report, Silicon Materials Task (Part 2) DOE/JPL 954331-76/3, July (1976).
5. V. P. Boldrev et al, Sov. Phys. Semicond., V11 No. 6 (1977).
6. C. S. Duncan, et al, Annual Report, Silicon Web Process Development, DOE/JPL-954654-79/2, April (1979).

7. ACKNOWLEDGEMENTS

We would like to thank the following individuals whose contributions have been important to the success of this program: D. N. Schmidt (cell processing and testing), B. F. Westwood (process experiments and photolithography, A. M. Stewart (material characterization and web growth), H. F. Abt (metallization), C. F. Seiler (device measurements), S. Karako (DLTS measurements), T. Zigarovich (mask preparation), D. Labor (manuscript preparation), and S. Farukhi (manuscript editing).

8. APPENDIX

Appendix 1. Ingot Impurity Concentration

Ingot Identification	Target Concentration $X10^{15}$ atoms/cm^3	Calculated Concentration $X10^{15}$ atoms/cm^3	Mass Spec. Analysis $X10^{15}$ atoms/cm^3
W-129-00-000 (7.6 cm.)	NA	NA	NA
W-130-00-000 (7.6 cm.)	NA	NA	NA
W-131-Mn-008 (7.6 cm.)	0.6	0.55	0.55
W-132-Ta-003	0.0002	0.0009	<0.5
W-133-00-000	NA	NA	NA
W-134-Ti-009	0.05	0.03	<0.25
W-135-Fe-005	1.0	0.78	<1.5
W-136-Fe-006	0.3	0.24	<1.5
W-137-Ti-010	0.21	0.21	<0.25
W-138-Mo-005	0.001	0.0008	<0.5
W-139-Mo-006	0.0042	0.0054	<0.5
W-140-Ti-011 (7.6 cm.)	0.18	0.18	<0.25
W-141-Mo/Cu-001	0.004/4.42	0.003/3.68	<0.5/4.00
W*-142-00-000	NA	NA	NA
W*-143-Ti-002	0.20	0.17	<0.25
W*-144-Mo-001	0.0042	0.0044	<0.5
W-145-W-001	0.001	0.00085	<0.15
W-146-Co-001	0.55	0.39	0.55
W-147-N/Ni-002	0.4	0.33	<1.5
W-148-N/Mn-002	0.60	0.76	0.55
W-149-N/Fe-003	0.60	0.58	<1.5
W-150-N/V-003	0.03	0.03	<0.15
W**-151-00-000	NA	NA	NA
W**-152-Ti-001	0.2	0.22	<0.25
W-153-N/Ti-003	0.01	0.017	<0.25
W-154-N/Cr-003	0.55	0.71	0.35
W-155-N/Mo-001	0.001	0.001	<0.50
W-156-N/Mo-002	0.004	0.003	<0.50

Appendix 1. Ingot Impurity Concentration (cont.)

Ingot Identification	Target Concentration $X10^{15}$ atoms/cm^3	Calculated Concentration $X10^{15}$ atoms/cm^3	Mass Spec. Analysis $X10^{15}$ atoms/cm^3
W-157-N/Ti/V-001	Ti: 0.10	0.08	<0.25
	V: 0.10	0.12	<0.15
W-158-N/Ti/V/Cr-001	Ti: 0.05	0.05	<0.25
	V: 0.05	0.05	<0.15
	Cr: 0.60	0.55	0.33
W-159-N/Cr/Mn/Ti/V-001	Cr: 0.4	0.35	0.20
	Mn: 0.4	0.32	0.25
	Ti: 0.02	0.02	<0.25
	V: 0.02	0.02	<0.15
W-160-Ti-001	0.2	0.17	<0.25
W-161-Ti-002	0.02	0.03	<0.25
W-162-Ni/Ti-001	Ni: 1.0	1.21	<1.5
	Ti: 0.2	0.16	<0.25
W-163-Ni/V-001	Ni: 1.0	1.01	<1.5
	V: 0.4	0.44	0.15
W-164-Ni/Mo-001	Ni: 1.0	1.23	<1.5
	Mo: 0.004	0.004	<0.5
W-165-Co-002	Co: 0.11	0.11	<0.55
W-166-Fe-007	Fe: 0.9	1.06	<1.5
W-167-Nb-001	Nb: Max	Processing	<0.15
W-168-Ph-002	31	NA	(105)$^+$
W-169-Ph-004	40	NA	(141)$^+$
W-170-Ph-005	56	NA	(150)$^+$
W-171-W-002	0.002	Incomplete	<0.15
W-172- Cu-006 (7.6 cm)	10	32	24

Appendix 1. Ingot Impurity Concentration (Cont.)

Ingot Identification	Target Concentration x 10^{15} atoms/cm^3	Calculated Concentration x 10^{15} atcms/cm^3	Mass Spec. Analysis x 10^{15} atoms/cm^3
W-173-Fe-008 (7.6 cm)	0.64	0.51	<1.5
W-174-Ta-004	0.004	0.0044	<0.50
W-175-W-003	0.0003	0.0003	<0.15
W-176-00-000	NA	NA	NA
W-177-N/Cr/Mn-001	Cr:1.0 Mn:1.3	1.20 1.26	1.0 2.7
W-178-N/Mn/Ti-001	Mn:1.0 Ti:0.1	0.86 0.08	2.8 <0.25
W*179-Ph-006	21	NA	(73)+
W*180-Ti-001	0.2	0.13	<0.25
W-181-Cr-006	1.0	1.04	1.0
W-182-Cr-007	0.25	0.37	0.65
W-183-Nb-002	20% Max.	Processing	<0.15
W-184-Pd-001	Max. Conc.	Processing	Processing
W-185-Cu/Ti-004	Cu:1.7 Ti:0.2	Processing Processing	Processing Processing
W-186-Co-003	0.01	Processing	Processing
W-187-Co-004	0.05	Processing	Processing

* Low resistivity p-type ingot ($\leq$ 1 Ω-cm).

** 30 Ω-cm p-type ingot.

\+ Value based on resistivity measurement.